NASA/CR—2004–XXXXXX

Design Of A High Efficiency Power Source (HEPS) Based On Thermoacoustic Technology

Michael Petach[1], Emanuel Tward[1], and Scott Backhaus[2]

[1]Northrop Grumman Space and Technology
Space & Electronics Group
One Space Park
Redondo Beach, CA 90278

[2]Los Alamos National Laboratory
Condensed Matter and Thermal Physics
MST-10, MS-K764
Los Alamos, NM 87545

January 2004

The NASA STI Program Office ... in Profile

Since its founding, NASA has been dedicated to the advancement of aeronautics and space science. The NASA Scientific and Technical Information (STI) Program Office plays a key part in helping NASA maintain this important role.

The NASA STI Program Office is operated by Langley Research Center, the lead center for NASA's scientific and technical information. The NASA STI Program Office provides access to the NASA STI Database, the largest collection of aeronautical and space science STI in the world. The Program Office is also NASA's institutional mechanism for disseminating the results of its research and development activities. These results are published by NASA in the NASA STI Report Series, which includes the following report types:

- TECHNICAL PUBLICATION. Reports of completed research or a major significant phase of research that present the results of NASA programs and include extensive data or theoretical analysis. Includes compilations of significant scientific and technical data and information deemed to be of continuing reference value. NASA counterpart of peer-reviewed formal professional papers, but having less stringent limitations on manuscript length and extent of graphic presentations.

- TECHNICAL MEMORANDUM. Scientific and technical findings that are preliminary or of specialized interest, e.g., quick release reports, working papers, and bibliographies that contain minimal annotation. Does not contain extensive analysis.

- CONTRACTOR REPORT. Scientific and technical findings by NASA-sponsored contractors and grantees.

- CONFERENCE PUBLICATION. Collected papers from scientific and technical conferences, symposia, seminars, or other meetings sponsored or co-sponsored by NASA.

- SPECIAL PUBLICATION. Scientific, technical, or historical information from NASA programs, projects, and missions, often concerned with subjects having substantial public interest.

- TECHNICAL TRANSLATION. English-language translations of foreign scientific and technical material pertinent to NASA's mission.

Specialized services that complement the STI Program Office's diverse offerings include creating custom thesauri, building customized databases, organizing and publishing research results ... even providing videos.

For more information about the NASA STI Program Office, see the following:

- Access the NASA STI Program Home Page at ***http://www.sti.nasa.gov***

- E-mail your question via the Internet to help@sti.nasa.gov

- Fax your question to the NASA STI Help Desk at (301) 621-0134

- Telephone the NASA STI Help Desk at (301) 621-0390

- Write to:
  NASA STI Help Desk
  NASA Center for AeroSpace Information
  7121 Standard Drive
  Hanover, MD 21076-1320

NASA/CR—2004–XXXXX

Design Of A High Efficiency Power Source (HEPS) Based On Thermoacoustic Technology

Michael Petach[1] , Emanuel Tward[1], and Scott Backhaus[2]

1
Northrop Grumman Space and Technology
Space & Electronics Group
One Space Park
Redondo Beach, CA 90278

2
Los Alamos National Laboratory
Condensed Matter and Thermal Physics
MST-10, MS-K764
Los Alamos, NM 87545

National Aeronautics and
Space Administration

Glenn Research Center
Cleveland, OH 44135

Prepared for NASA Glenn Research Center
under Contract NAS3-01103

January 2004

Acknowledgments

The authors would like to acknowledge the assistance of those individuals who aided in the preparation of this document. Scott Backhaus of Los Alamos Laboratories provided the crucial thermodynamic modeling, insight and hardware that was key to obtaining the source data. Paul Bailey was central to overcoming key alternator design and assembly hurdles. Carl Carlson's troubleshooting skills were invaluable in insuring that the hardware worked as designed once assembled for test.

Available from:

NASA Center for AeroSpace Information
7121 Standard Drive
Hanover, MD 21076-1320
301-621-0390

National Technical Information Service
5285 Port Royal Road
Springfield, VA 22161
703-605-6000

January 2004

Northrop Grumman Space and Technology
Space & Electronics Group
One Space Park
Redondo Beach, CA 90278

Design Of A High Efficiency Power Source (HEPS) Based On Thermoacoustic Technology

Final Report

Michael Petach[1], Emanuel Tward[1], and Scott Backhaus[2]

1
Northrop Grumman Space and Technology
Space & Electronics Group
One Space Park
Redondo Beach, CA 90278

2
Los Alamos National Laboratory
Condensed Matter and Thermal Physics
MST-10, MS-K764
Los Alamos, NM 87545

NASA Contract No. NAS3-01103, CDRL 3f

NGST Sales Number 1C319

Prepared by
Michael B Petach
Project Manager
Phone: 310-812-0384
Email: michael.petach@ngc.com

January 2004

Table Of Contents

List Of Figures

List Of Tables

Summary

A traveling-wave thermoacoustic power converter that generates electricity from heat was developed and tested. Models were developed, and trade studies were performed to design a power conversion system aimed at the ~100-W radioisotope-powered deep-space and Mars Lander Missions.

The power converter design incorporates a thermoacoustic driver that converts heat to acoustic power without any moving parts. The acoustic power is used to drive a pair of flexure-bearing-supported pistons connected to voice coils in a vibrationally balanced pair of moving coil alternators, which produces ac electrical power.

An existing 1-kW thermoacoustic heat engine design was scaled down to ~100 Watts. Several of these small ~100-W heat engines were built and tested as components. Component tests of the ~100-W thermoacoustic driver demonstrated very good thermal-to-acoustic efficiency. An existing NGST flight-like compressor was modified to match to the thermoacoustic driver's acoustic impedance requirements and act as an alternator. The combined heat engine and alternator demonstrated efficient thermoacoustic production of electrical power from a simulated radioisotope heat source using hardware similar to that of flight-proven cryocoolers. The power converter performance was characterized as a function of heat input (and thus alternator stroke) at fixed hot-end temperature and fixed reject temperature. Additional characterization was done varying reject temperature while maintaining fixed hot-end temperature and fixed alternator stroke The thermoacoustic power converter successfully produced over 50 Watts of electrical output power at up to 18% system efficiency. This is the first known successful implementation of traveling-wave, thermoacoustic-to-electrical power conversion technology and is just a first step toward a space-qualified, high-efficiency power source based on thermoacoustic technology. Modeling, analysis and diagnostic testing performed during this contract have identified potential system improvements to the efficiency and total power output.

Background

A thermoacoustic space power converter is being developed in order to provide an efficient, a low-mass power source for deep-space and Mars Lander missions. The converter is being designed to convert heat produced by the radioactive decay of ^{238}Pu contained in a General Purpose Heat Source (GPHS) to electricity for powering a spacecraft or a Mars rover. The well-developed Radioisotope Thermal Generator (RTG) technology currently used on NASA missions such as Cassini, and Voyager have demonstrated long life. However, RTGs have a heat-to-electrical power conversion efficiency of ~8% and require a relatively large quantity of ^{238}Pu per unit of electrical output power. Increasing the converter efficiency is a desirable goal in order to reduce the quantity of ^{238}Pu that is launched for reasons of safety and ^{238}Pu availability. NASA is seeking to develop alternative highly reliable (>100,000 hour lifetime), higher specific power (~10 W/kg), and more efficient (13%-25%) thermal-to-electric converters in the 100-W_e power range (Mondt, 2001).

A Stirling Radioisotope Power Source (SRPS) is being developed by the DoE and NASA as an alternative to RTG's because of its higher efficiency (>20%) (Cockfield, 2002). This dynamic

power converter incorporates a Stirling heat engine that produces an acoustic pressure wave to drive a piston in a linear alternator. The linear alternator produces the electricity.

A thermoacoustic radioisotope power source (TARPS) is a dynamic power converter that offers considerable potential benefit in reliability, producibility, efficiency and specific power (Backhaus, 2002). Like the SRPS, the converter uses a linear alternator. However, the TAPRS linear alternator is derived from flight-proven, high-efficiency linear compressors used in space-based cryocoolers (Tward, 2001). Unlike other dynamic converters, such as the Stirling heat engine and the turbo Brayton heat engine, the hot thermoacoustic driver has no hot moving parts, a feature that eliminates major failure modes and manufacturing difficulties and contributes to system safety. Recent innovations in thermoacoustics have resulted in demonstrated thermal-to-PV power conversion efficiencies of up to 30%. This high thermal-to-acoustic conversion efficiency can be utilized to produce a low-mass, reduced-^{238}Pu-requirement converter with high efficiency.

We have estimated the mass of a "flight-weight" 100-W_e TARPS to be 13.9 kg with a beginning of life (BOL) specific power of 8.3 kg/W_e .

Thermoacoustic Radioisotope Power Source Overview

A Thermoacoustic Radioisotope Power System integrates the GPHS, the converter, and the electronics into a complete thermal/mechanical/electrical design. Figure 1 shows a TARPS block diagram. The GPHS provides the heat required to drive the heat engine. The passive thermoacoustic heat engine produces an acoustic pressure wave that drives a pair of opposed, non-wearing pistons. The gas clearance seal between the moving pistons and stationary cylinders is maintained by radially stiff flexures. Each piston is attached to a voice coil in the vibrationally balanced linear alternator. The alternator generates an ac electric wave that the electronics convert to 28-Vdc power. The electronics also provide control functions to the alternator including load switching.

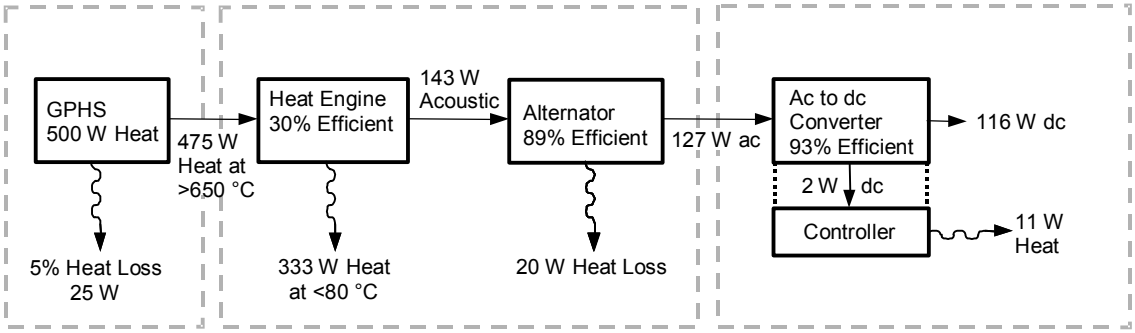

Figure 1. System diagram illustrating the goals of a TARPS system

Figure 1 also shows projected component efficiencies and the system heat and power flows. The 30% heat engine efficiency has been measured for a 1-kW unit (Backhaus, 2000) and has been modeled for a 100-W unit. The 89% alternator efficiency is based on the measured efficiency of NGST's AIRS cryocooler compressor operating at 100 W. Two of these units are currently in orbit. The 93% ac-to-dc converter efficiency is based on NGST's current miniaturized cryocooler

flight dc-to-dc converters that achieve >91% efficiency in 200-W systems. Since to some extent the efficiency is determined by the mass of magnetics in the converter, we assume that for the same mass, the lower power 100-W ac-to-dc converter can achieve the additional 2%. The rejected heat must ultimately be radiated to space. The hot end temperature of the heat engine is potentially limited by long-term material creep problems of conventionally available Inconel materials. For this reason we assume a 650 ^{o}C upper temperature which is well below the capability of the GPHS unit. The efficiency of the system and the output power increases with the temperature difference between the high and low temperatures. For this reason, future improvements can come from the use of other materials (or mechanical designs) that allow higher input temperature.

The initial TARPS conceptual design (Figure 2) incorporates a vibrationally balanced alternator that is integrated with the passive heat engine and is heated by the GPHS. The GPHS is contained in a thermally insulated gas tight housing and is thermally coupled to a flat-plate hot heat exchanger. The housing around the hot end can be backfilled with inert gas to prevent oxidation of hot surfaces prior to launch and can be vented in orbit or to the Martian atmosphere on a lander. The single low-temperature thermal reject surface also serves as the mounting surface. The TARPS may be bolted directly to a radiator or heat pipes can be used to transport heat to other components on the spacecraft. If required, the electronics can be located on the spacecraft. This integral configuration allows considerable size, mass, and structural savings.

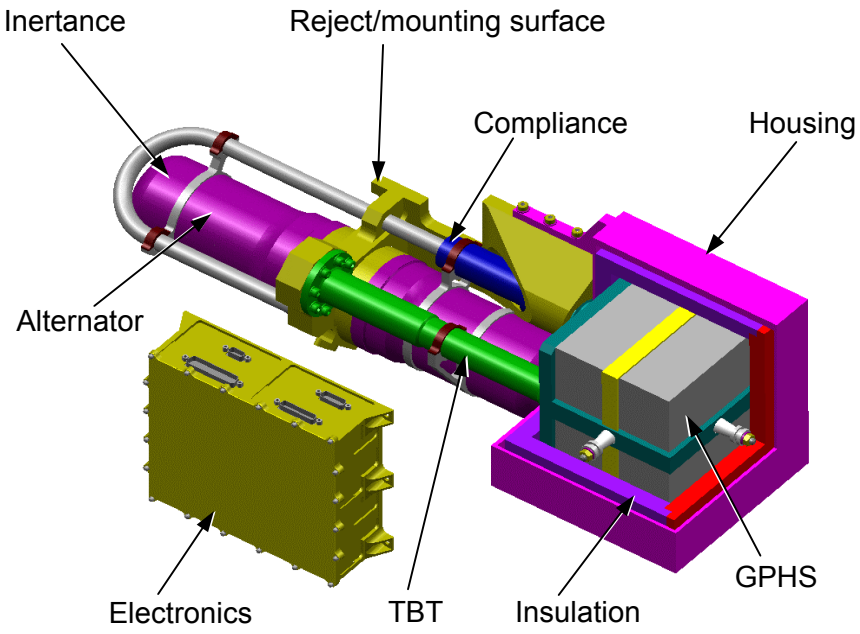

Figure 2. Thermoacoustic Radioisotope Power System Incorporating the Initial Thermoacoustic Power Converter Concept

The thermoacoustic power converter consisting of the heat engine and balanced alternator is shown in Figure 3.

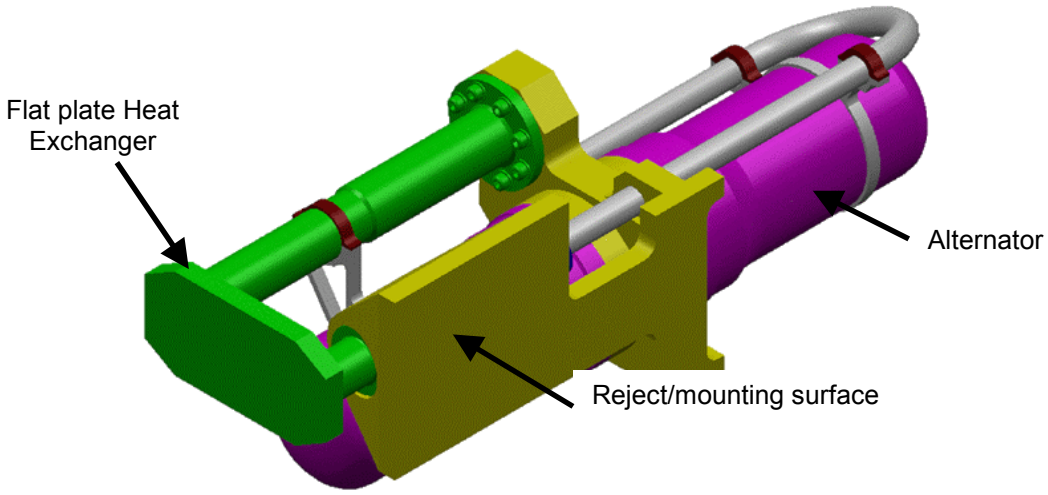

Figure 3. Initial Thermoacoustic Power Converter Concept

Since the heat engine has no moving parts, its geometry can be very flexible. The initial design shown in Figure 3 has been chosen so that the hot end of the Thermoacoustic-Stirling Heat Engine (TASHE) is flat and exposed on one end. This configuration allows for a simple thermal and mechanical interface with the GPHS. In principle, solid conduction from the GPHS to the hot heat exchanger could be used to couple the heat into the TASHE. An interface of this type should not require any additional metal to transport the heat to the TASHE or to support the GPHS. This provides an additional mass savings when the converter is integrated with the rest of the power system. With no moving parts in the hot end of the TASHE, creep of the hot end material induced by the high temperatures and high internal pressure will not cause any performance issues due to the loss of a critical tolerance. The TASHE is described in greater detail in the next section of this report. Essentially, it is composed of a looped flow path filled with high-pressure helium. The loop contains the regenerator, heat exchangers, and other ductwork necessary to force the helium gas in the regenerator to oscillate and execute a Stirling-like thermodynamic cycle when heat is applied.

The oscillating flow impinges on the opposed pair of pistons in the linear alternator. The linear alternator is derived from our low-mass, flight-proven cryocooler compressors as shown in Figure 4. The alternator converting the acoustic power to electrical output is very similar to eight in-orbit, vibration-balanced, long-life, non-wearing, flexure, linear cryocooler compressors built by NGST. These moving coil compressors (and alternators) are scalable as illustrated by the three back-to-back cryocooler compressors shown in Figure 4. The compressors in the Figure accept input powers of 80, 200 and 800 Watts respectively.

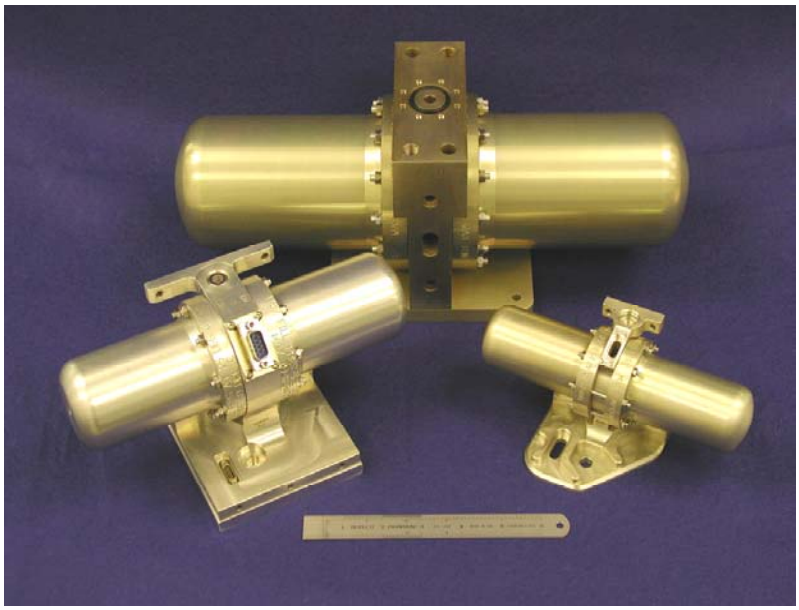

Figure 4. Cryocooler Compressors

The compressor/alternators are very small with low mass. The balanced 80-W unit shown has a mass of 1 kg. The operational difference is that in the case of the cryocooler, an electrical sine wave is the input and the moving piston produces acoustic power. In the heat engine, acoustic power is the input to the piston and electrical energy is the output. The chief difference in the machines is that, per unit of power the required, pressure amplitude and swept volume is larger for the TARPS than for the cryocooler. This allows the potential for some weight savings in the alternator magnetic circuit, but this is offset by the requirement for a larger piston. In the typical back-to-back alternator in Figure 4, the two halves are driven in opposition by the acoustic pressure wave introduced at the port in the center plate. Each half contains a piston attached to a voice coil mounted on flexure springs. The flexures maintain a non-contacting, non-wearing, gas seal between the piston and the cylinder. The moving coil and piston structure is resonant with the gas "spring" formed by the thermoacoustic driver and generates electrical power as it moves in the magnetic field of the motor stator. NGST pulse tube cooler units incorporating compressors based on this principle have been operating continuously in space without degradation for the past five years. The alternator and TASHE are designed to be resonant at the design frequency and have matched swept volume and pressure ratio.

We have estimated the end-to-end mass based on breadboard components, specific power and conversion efficiency of a complete TARPS that is similar to the concept shown in Figure 2. The mass including 12% contingency is 13.9 kg. The end-to-end conversion efficiency is 23.2% (116 W/500 W) as shown in Figure 1. The power converter component has an efficiency of 26.7% and a mass of 4 kg. The resultant specific power for the complete TARPS at beginning of life is 8.3 W_e/kg.

Thermoacoustic Stirling Heat Engine Modeling Details

The power converter was been modeled and analyzed with Los Alamos National Lab's DeltaE computer program (Ward, 1994), a first-principles accurate modeling program that predicts how a given thermoacoustic engine and alternator will perform. The code numerically integrates a one-dimensional wave equation appropriate to a user-defined geometry in a user-selected gas or liquid. DeltaE is capable of handling complex geometric configurations and specialized acoustic

elements, including resonators, duct networks, and complete thermoacoustic engines such as prime movers or electro-acoustically-driven refrigerators. The DeltaE model for the combined heat engine and linear alternator developed for this program contains elements describing every mechanical part in the system. In cases where the geometric description of a mechanical element was not possible (for example in describing the alternator windage), subcomponent test data was used to provide a model element, which was incorporated into the overall DeltaE model. DeltaE's multivariable mapping capabilities allowed extensive design trades to be investigated,which helped in accurately designing an apparatus to achieve desired performance. This model also helped troubleshoot the hardware during the development stage, and interpret the final test results

Thermoacoustic-Stirling Heat Engine Detailed Description

Thermoacoustic engines convert high-temperature heat into acoustic power without using moving parts. Recent innovations in thermoacoustics have allowed these engines to utilize the more efficient Stirling thermodynamic cycle (Backhaus, 2000). The result has been an increase in thermal-to-acoustic conversion efficiency from ~21% to 30%. A large Thermoacoustic-Stirling Heat Engine (~1kW of PV power) has demonstrated 30% efficiency.

The layout of the TASHE is shown in Figure 5. Essentially, it is composed of a looped flow path filled with 52-bar helium. The loop contains the regenerator, heat exchangers, and other ductwork necessary to force the helium gas in the regenerator to execute the Stirling cycle (Backhaus, 2000). The mass of the TASHE up to the resonator/alternator interface is approximately 900 grams. The total mass was measured after several pieces of instrumentation were installed, but before a final closure weld was made. At this 100-W scale, the TASHE contributes less than 10% of the mass in the 10 W/kg space power system desired by NASA (Mondt, 2001). Additional mass savings are possible. If designed for a flight system instead of laboratory convenience, much of the instrumentation and bolting flanges would be removed. Also, much of the extraneous metal in the TASHE could be removed, and aluminum could be substituted for several of the stainless steel components.

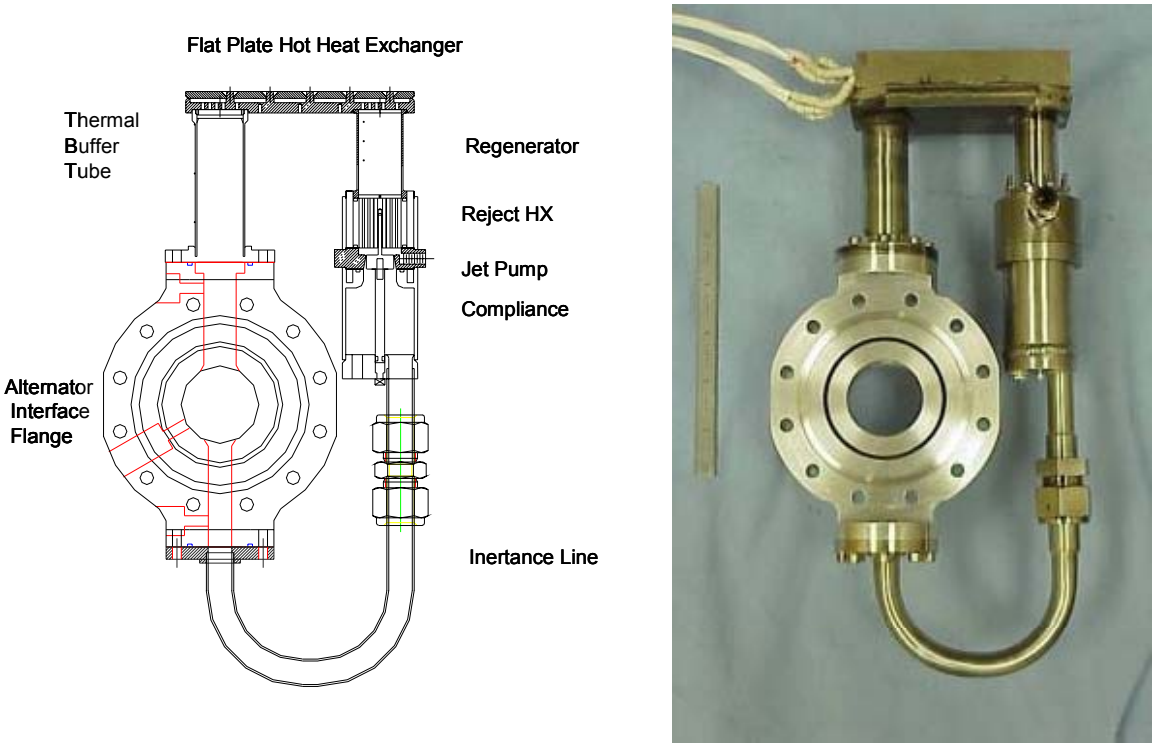

Figure 5. Cross Section of the TASHE including flange to connect to alternator

In Figure 5, the top of the loop is a 2-mm gap between two parallel plates forming the hot heat exchanger. The plates, shown in Figure 6, are made of Inconel 625, and are 10.5-cm long and 5.2-cm wide (into the page in Figure 5) . High-temperature heat enters the system by solid conduction through the top plate. There are many 3.5-mm-diameter pins machined into the bottom plate and welded into holes through the top plate. These are not intended to increase the heat transfer area. They simply act as supports to keep the thin top plate from bowing outward under the action of the 52-bar pressure. The high-temperature heat is generated in a metal heater block that simulates the GPHS. The nickel heater block, which is brazed to the top surface of the hot heat exchanger, has four electrical cartridge heaters embedded in it.

Since the TASHE has no moving parts, its geometry can be very flexible. This is very beneficial when interfacing to a heat source such as a GPHS that has a flat heat transfer surface. The design shown in Figure 5 has been chosen so that the hot end of the TASHE is flat and exposed on one end. This configuration allows for a simple thermal and mechanical interface with the GPHS. In principle, solid conduction from the GPHS to the hot heat exchanger could be used to couple the heat into the TASHE. An interface of this type should not require any additional metal to transport the heat to the TASHE or to support the GPHS. This provides an additional mass savings when the converter is integrated with the rest of the power system. With no moving parts in the hot end of the TASHE, creep of the hot-end material induced by the high temperatures and high internal pressure will not cause any performance issues due to the loss of a critical tolerance. A finite element analysis of the combined thermal and pressure stresses in the hot end of the TASHE (Appendix A) shows that the NASA GRC 100,000-hour durability requirement can be readily met

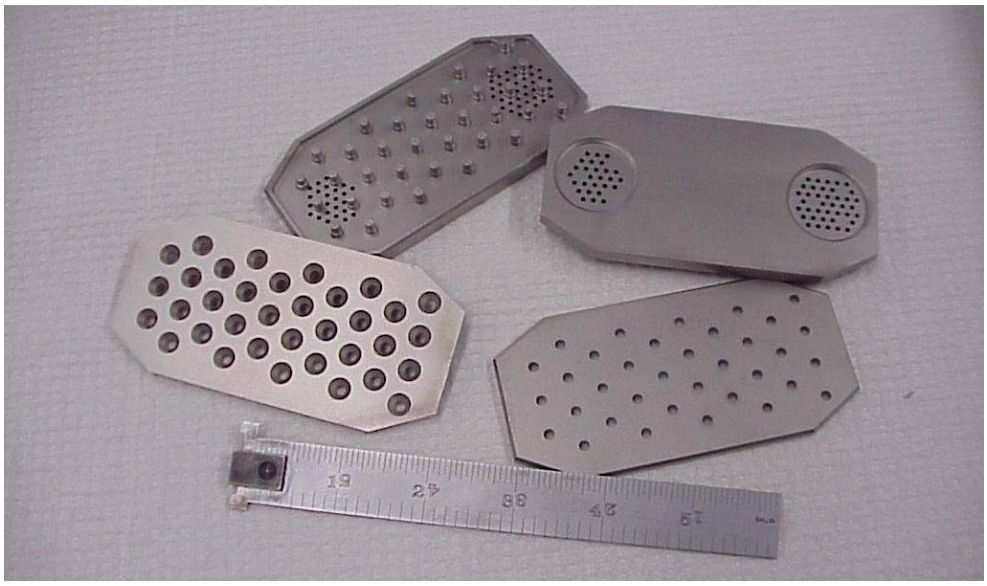

Figure 6. Upper and lower plates of the Flat-Plate Hot Heat Exchanger

Proceeding down the right leg of the loop is the regenerator. It is composed of a stack of stainless-steel screens packed into a thin-wall Inconel-625 tube approximately 4-cm long. Below the regenerator is the main ambient heat exchanger. It is an aluminum cylinder with 48 1.6-mm-diameter holes drilled through. The waste heat rejected by the TASHE through this heat exchanger is finally carried away by cooling water flowing through an annular passage around the outside of the heat exchanger.

In the left leg of the loop below the hot heat exchanger is the thermal buffer tube (TBT). It is a thin-wall Inconel-625 tube. The TBT allows acoustic power to flow away from the hot heat exchanger while thermally isolating the hot end from ambient temperature. To avoid large convective heat leaks, it is crucial that the flow in the TBT remain thermally stratified. Flow straighteners are placed at either end of the TBT to suppress any jetting out of the adjacent heat exchangers that would cause mixing of hot and cold gas. The flow straightener at the ambient end of the TBT acts as a heat exchanger that restricts the thermal gradient to the TBT and protects the linear alternator from the high temperatures of the hot heat exchanger.

The heat exchangers, regenerator, and TBT described above form the thermodynamic section of the TASHE. A crucial acoustic network is formed by the open volume, or compliance, below the main ambient heat exchanger and the inertance tube that connects the ambient end of the TBT to the compliance. This network generates pressure and velocity oscillations in the regenerator that drive the gas through the Stirling cycle (Backhaus, 2000). The compliance has a volume of approximately 30 cm^3. The inertance is simply a tuned tube that is connected to the compliance at one end and the TBT (via the compression space) at the other end. As the gas oscillates back and forth through the inertance, the compliance is pressurized and depressurized generating pressure oscillations in the regenerator. Also, the gas in the inertance must accelerate during the oscillations, and the inertia of the gas creates an oscillating pressure drop across the inertance. This pressure drop also appears across the regenerator, and it drives the oscillating velocity in the regenerator. The operation of the network can loosely be compared to that of a displacer piston in a free-piston Stirling engine. A detailed description of how this network operates can be found elsewhere (Backhaus, 2000).

The final component in the loop is located between the main ambient heat exchanger and the compliance. Called a "jet pump", it is an annular diffuser with the small end facing the main ambient heat exchanger. The edges of the small-end opening are radiused while the large-end opening is left sharp. The area of the small-end opening is adjustable by moving the central plug in the axial direction. The asymmetry of the flow out of the small end creates an adjustable time-averaged pressure drop that generates a steady flow around the TASHE's loop. This flow is used to cancel a parasitic steady flow around the loop generated by acoustic streaming. Without the action of the jet pump, the parasitic streaming flow would cause a convective heat leak on the hot heat exchanger lowering the efficiency of the TASHE. A detailed description of this phenomenon can be found elsewhere (Backhaus, 2000).

As the TASHE development progressed through three different versions, the instrumentation changed as well. Here, we describe the instrumentation of the final version that was used in the TASHE/alternator integrated testing. The TASHE is instrumented with pressure sensors and type-K thermocouples. The pressure sensors are located in the compliance, between the jet pump and cold heat exchanger, and at the junction between the inertance and TBT. These sensors measure the pressure drop across three key elements in the TASHE: the jet pump, regenerator, and inertance. If these pressure drops agree with numerical calculations, the actual oscillating velocities in the TASHE are assumed to be close to the calculated velocities.

Thermocouples are placed in several locations around the loop. Five are spot welded at equally-spaced intervals along the regenerator housing. These thermocouples are used to determine what jet pump setting suppresses the parasitic steady flow around the TASHE's loop (Backhaus, 2000). When the parasitic flow is stopped, the temperature profile in the regenerator is nearly linear. Four thermocouples spot-welded to the outside of the TBT serve a similar purpose. Any net steady flow around the loop will affect the temperature profile in the TBT. Also, acoustic streaming cells confined to the TBT (Olson, 1997) will modify its temperature profile. This second type of streaming will also cause a heat leak on the hot heat exchanger lowering the efficiency of the TASHE. The measurement of the temperature profile in the TBT helps to determine if these effects are significant. To analyze the effectiveness of the hot heat exchanger, there are five thermocouples touching the outer metal surface. They are distributed along the centerline of the plates that extends from the regenerator to the TBT. In early versions of the TASHE, two thermocouples were placed at either edge of the hot heat exchanger plates halfway between the regenerator and TBT and one in the center of the lower plate to verify that there were no hot spots due the oscillating flow not accessing all areas of the heat exchanger. Finally, there is a thermocouple placed at the OD of the main ambient heat exchanger that is used to analyze the effectiveness of this heat exchanger.

Initial TASHE-Component Development Tests

To make rapid progress, the TASHE is first tested on an acoustical resonator that mimics both the reactive and resistive properties of a linear alternator attached to an electrical load. The resonator has a variable acoustic load to allow the TASHE performance to be mapped as a function of pressure amplitude. A set of pressure sensors in the resonator and variable acoustic load allow measurement of the amount of acoustic power flowing into the resonator. This is the same power that impinges on the face of the linear alternator's piston. A description of this measurement technique can be found elsewhere (Backhaus, 2000 and Fusco, 1992). For unknown reasons, this measurement technique failed to provide accurate acoustic power data. It is believed that the theory behind the measurement is inadequate for a resonator with a small diameter as used in this

program. Therefore, rigorous testing of the TASHE component on a resonator was not possible. However, when changes to the TASHE configuration were made, relative tests could be performed to see if the changes resulted in a performance improvement. This initial testing demonstrated that a low-mass, 100-Watt TASHE with good efficiency was possible.

TASHE Temperature Profiles

Figures 7 and 8 show the test data from the first of three TASHE configurations tested during this program. Figure 7 shows the temperature distribution in the regenerator and TBT as well as the temperature of the hot and cold heat exchanger metal. As found previously, the TASHE delivers the most power to the resonator when the jet pump small-end area is adjusted so that the three measured temperatures in the regenerator fall along a straight line (Backhaus, 2000). In this condition, the jet pump is generating the amount of steady flow necessary to cancel the parasitic streaming flow and eliminate any potential convective heat leaks on the hot heat exchanger. Numerical calculations (Ward, 1994) confirm that when there is no net steady flow around the loop, the axial temperature profile along the regenerator is nearly linear.

Also, if there is no boundary-layer streaming or any other mixing processes occurring in the TBT (Olson, 1997), numerical calculations indicate that its temperature distribution should be nearly linear as well. The three TBT profiles shown in Figure 7 show small deviations from linear. These could be due to a small amount of boundary-layer streaming, inadequate flow straightening at the TBT ends, or possibly a radiation heat leak from the hot heat exchanger. However, at this early stage of testing, it is apparent that the TBT is performing nearly as expected, and these small deviations from the numerical predictions are not a concern.

In the hot heat exchanger section of Figure 7, the open symbols connected by lines are the measured temperatures on the top surface of the heat exchanger along an axis connecting the centerlines of the regenerator and TBT. For the data at the highest temperature, approximately 80 Watts of heat is transferred through the top plate. At these power levels, the temperature along this axis is fairly constant showing an ~20 ^{o}C variation from the midpoint to the location over the regenerator centerline. At higher power levels, this variation will increase due increased heat transfer, but the oscillating gas displacement will increase as well. The second effect will tend to reduce the temperature variation. Two additional thermocouples are placed at the transverse edges of the heat exchangers halfway between the regenerator and TBT. The crosses in Figure 2 indicate their average temperature. These data show that there is very little temperature variation in the direction transverse to the oscillating flow. This provides evidence that the oscillating flow is accessing all of the surface area in the hot heat exchanger even though the diameter of the regenerator and TBT (~2 cm) is smaller than the width of the heat exchanger (~ 5 cm, the depth into the page in Figure 5). With the flow accessing all of the surface exposed to the heat source, concerns about hot spots and associated pressure vessel failures are reduced. The final open symbol, which is not connected by a line, is the temperature at the center of the bottom plate. With very little heat transfer occurring between the oscillating gas and the bottom plate, this temperature is very close to the gas temperature.

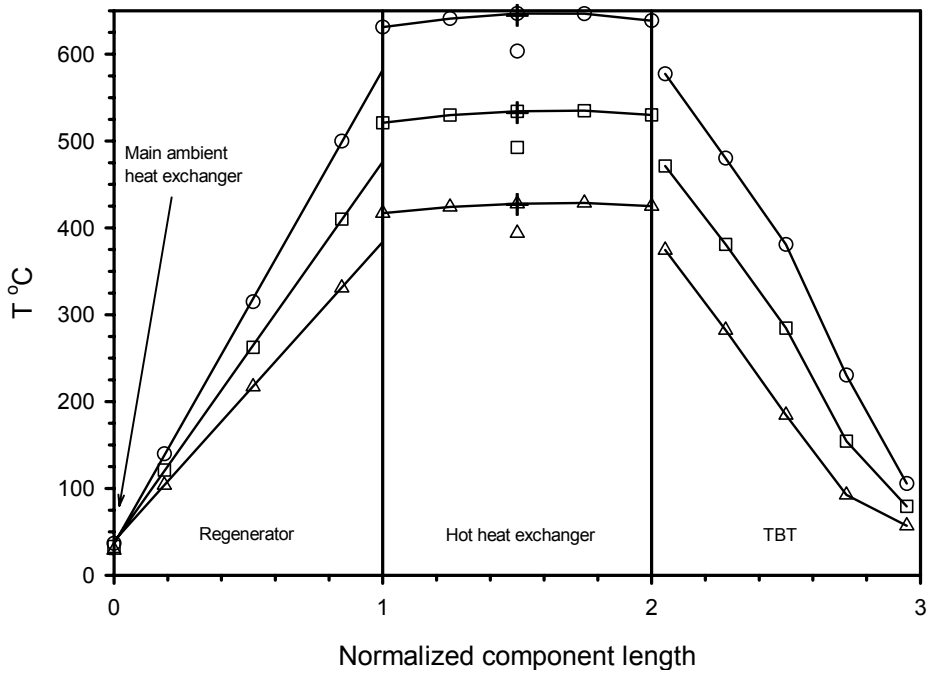

Figure 7. Temperature Distribution Through the TASHE.

The open circles, squares, and triangles are the measured temperatures at three different hot end temperatures at an oscillating pressure amplitude of approximately 150 kPa (~25% of design amplitude). The jet pump has been adjusted to ensure a linear temperature distribution in the regenerator. The open symbol in the hot heat exchanger section not connected by a line is the temperature of the hot heat exchanger bottom plate. The three crosses are the temperature at the edges of the heat exchanger plates for the different hot end temperatures. The straight lines in the regenerator section are least-squares fits to the 3 data points in that section. Although each section of the TASHE represented above is of different length, each length has been normalized to 1 to aid in the presentation of the data.

A straight line fit to the three temperatures in the regenerator is used to extrapolate the gas temperature at the hot and ambient ends of the regenerator. The extrapolated gas temperature at the ambient end is approximately 5 ^{o}C higher than the metal temperature at the OD of the main ambient heat exchanger. This gas-metal temperature defect is inline with expectations at these power levels. At the highest hot-end temperature, the extrapolated hot-end temperature is approximately 50 ^{o}C cooler than the hot heat exchanger top plate. The measured temperature defect is significantly higher than expected at these power levels. Part of this difference may be due to the positioning of the thermocouples. Only the very end of the thermocouple sheath actually touches the top plate. The location of the thermocouple junction, which is slightly removed from the end of the sheath, may be positioned in the cement which bonds the nickel heater block to the top plate. This would lead to an erroneously high temperature reading. In future tests, steps will be taken to ensure the thermocouple is reading the temperature of the top plate.

TASHE Pressure Drops

With the temperature distributions around the TASHE loop adjusted properly, the pressure drops across the various components are measured. Figure 8 shows the measured and numerically calculated pressure drop across the regenerator, jet pump, and inertance at an acoustic pressure amplitude of 150 kPa. There is reasonable agreement between the measured and calculated total pressure drop across the inertance. This gives confidence that the numerical calculation is accurately predicting the oscillating velocity throughout the TASHE. The main discrepancy is in

the pressure drop across the jet pump. This may be due to an alternate sensor mounting technique used due to the small size of the TASHE. However, the agreement of the total pressure drop with predictions is adequate for this component testing.

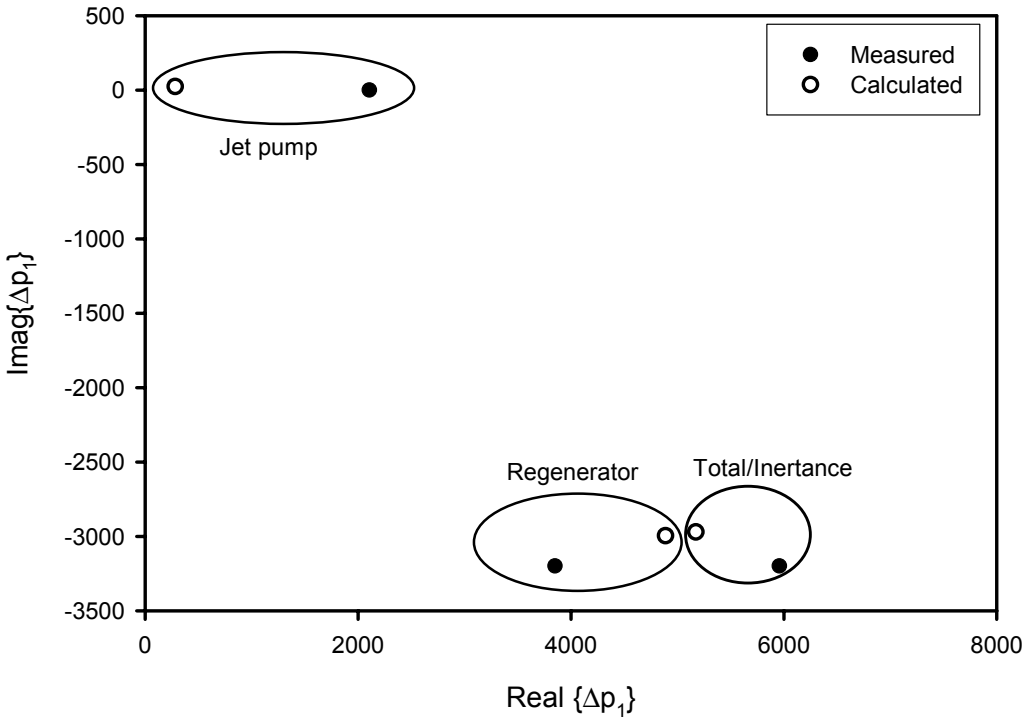

Figure 8. Acoustic Pressure Drops. Pressure drops across the regenerator, jet pump, and total drop across the inertance tube measured and calculated at an oscillating pressure amplitude of 150 kPa (~25% of design amplitude).

Alternator Description and Background

The resources available in this contract did not allow an optimized alternator to be designed and built. Analysis and scaling indicated, however, that an existing High Efficiency Cryocooler (HEC) compressor could be modified to accommodate the acoustic impedance requirements of the thermoacoustic heat engine and act as a test-bed alternator. The HEC compressor is a flight-qualified, 200-Watt-class cryocooler compressor. It is a moving-coil, permanent-magnet design with clearance seals and flexure springs based on the "Oxford" design. Its characteristics are described in greater detail elsewhere (Tward, 2001).

The compressor had to be modified because the TASHE presents a significantly different acoustic impedance than the pulse tube cryocooler for which this compressor was designed. The resonance condition for combined TASHE and alternator operation is given by

$$\left|\mathrm{Im}(p_1 / U_1)\right| = m\omega / 2A^2 \ ,$$

where p_1 and U_1 are the TASHE acoustic pressure and volumetric flow rate amplitudes, m and A are the moving mass and piston area of one half of the opposed-pair alternator, and ω is the operating frequency of both the TASHE and alternator. U_1 is also the alternator volumetric

velocity given by ωAX where X is the alternator stroke amplitude. Thus both the TASHE and alternator must share ω and A.

In addition to a different acoustic impedance, the operating parameters for the HEC-style alternator connected to the TASHE are quite distinct from those associated with the pulse tube cryocooler for which it was originally designed. The aspects of the TASHE application that give rise to the most significant differences are:

- The swept volume is significantly higher (21 cc *vs*. 6 cc)
- The peak-to-peak pressure is a factor of two higher (6 bar *vs.* 3 bar)
- The mean pressure is higher (750 psig *vs.* 500 psig)
- The maximum operating frequency is higher (125 Hz *vs.* 70 Hz).
- The maximum ambient-end operating temperature is higher (up to 120 ^{o}C *vs.* 40 ^{o}C).
- This particular TASHE application requires tolerance of high levels of ionizing radiation.

In the TASHE, the phase angle between pressure and volumetric velocity is much smaller than in a typical pulse tube cryocooler, thus the pressure amplitude, volumetric velocity, and frequency are much higher than those of the cyrocooler. In a nutshell, the ratio of power stored in the piston motion to the power extracted from the piston is much higher in the TASHE than in the cyrocooler. To accommodate the TASHE, the piston diameter had to be increased by nearly a factor of two while maintaining the same or better clearance seal gap dimensions. In addition, a new pressure vessel was required to accommodate the higher mean pressure, as well as to accommodate an LVDT position sensor. Additional electrical feedthroughs were required to accommodate the LVDT position sensor, which is vital to the interpretation of the thermoacoustic generator development tests but is not part of an HEC compressor. The motor portion of the HEC compressor, which is designed for up to 200-Watt operation at nominally 70 Hz, was left unchanged. This meant that the alternator operating temperature range was limited to less than 50 ^{o}C and that the alternator was operating somewhat off its electrical design point and well above its mechanical loss design point.

Analysis and scaling of existing HEC compressor-component test data indicated that the motor windage, magnetic hysteresis, seal blow by, and pressure vessel losses would grow after modification to accommodate the acoustic impedance requirements of the thermoacoustic heat engine, but would still allow it to act as a test-bed alternator.

An exiting HEC compressor was modified by adding much lager pistons and LVDT sensors, as shown in Figure 9. An additional consequence of these modifications was that an extended piston housing, more electrical feedthroughs, and larger pressure vessels were required for the test alternator. Figure 10 shows a photo of the alternator with the pressure vessel removed.

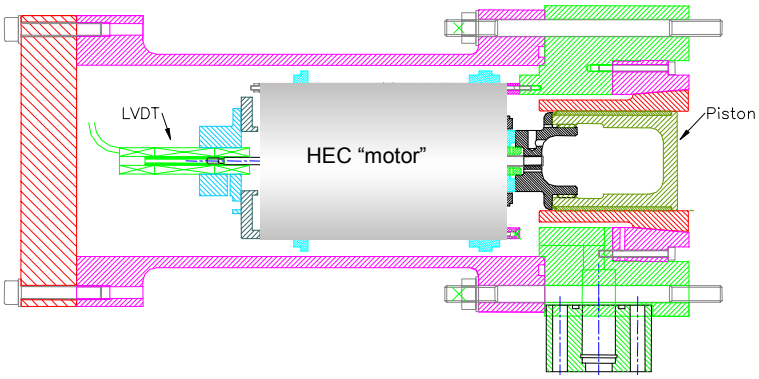

Figure 9. Alternator cross section

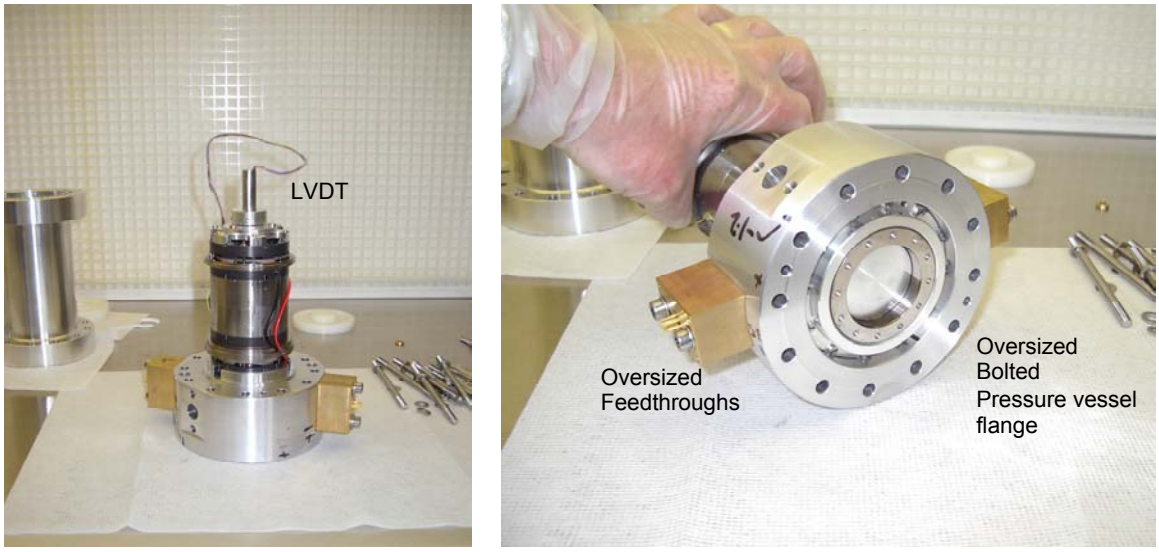

Figure 10. Alternator during assembly showing the LVDT sensor, large pistons, oversized flanges, and feedthroughs

Alternator Component Tests

During the process of modifying the existing NGST HEC compressor, several subassembly component tests were performed to validate key performance requirements and to measure some loss terms that are very difficult to predict analytically, such as motor windage and gas spring losses in the pressure vessel space. Before the new pistons were put onto the motors, a loss test was performed by operating the motors inside the pressure vessels at a variety of fill pressures and frequencies. This allowed the windage and the eddy current hysteresis losses to be estimated, and they were found to be acceptable for a test alternator. After the pistons were installed, the clearance seal gaps were measured via a pressure drop versus flow rate test. The flow measurement corresponded to a 9-10 μm radial gap, which is at or below the requirements for a flight system. After the alternator was fully assembled, it was tested as a compressor operating into a "dead volume," which is a minimum surface-area volume matched to the effective volume of the thermoacoustic heat engine. Thus, the HEC acting as a compressor into dead volume resonates at approximately the same frequency and has approximately the same pressure *vs.* stroke characteristics as the as when acting as an alternator attached to a TASHE.

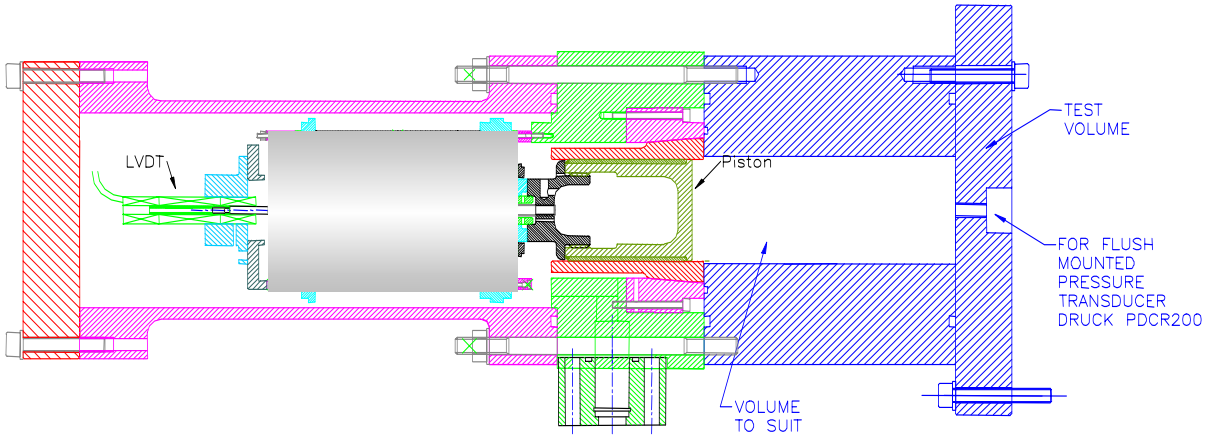

Figure 11. Alternator dead volume test configuration, with test volume to match TASHE effective volume, but with minimum surface area to minimize losses in the test volume compression space

This "dead volume" test approximately matched the fill pressure, frequency, stroke amplitudes, and pressure amplitudes expected during operation as an alternator driven by the TASHE. The total input power required to drive the compressor at a given stroke and pressure was measured, as was the I^2R loss in the coil. The shaft power could then be determined by subtracting the I^2R loss and calculated gas-spring hysteresis losses from the total input power. The result, which is shown in Figure 12, is the shaft power required to overcome the seal loss, motor windage, magnetic hysteresis, and back-volume gas-spring hysteresis losses as a function of stroke. This test checks that the subcomponent tests have identified all the loss terms.

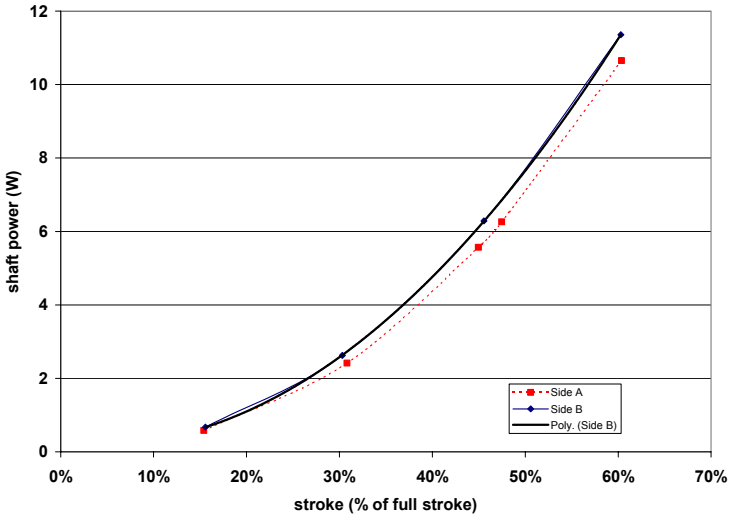

Figure 12. Alternator dead volume test shaft power vs. stroke

It was evident that the gas-spring hysteresis in the pressure vessel is a significant contributor. The increased losses are due to a higher pressure amplitude in the pressure vessel (from large piston displacement) and additional surface area (due to the addition of the LVDT) compared to normal pulse-tube-cryocooler operation. The loss was low enough to allow the alternator to be useful as a proof-of-concept test bed, but severely limited the efficiencies achievable at higher strokes. Additionally, the increased piston area and higher pressure amplitudes resulted in large piston position offsets at higher strokes which imposed a stroke constraint that limited the operating range available from the modified compressor. Nonetheless, these modified compressor component tests all indicated that the HEC alternator would be sufficient as a proof-of-concept test bed.

Combined Heat Engine and Alternator Test

The TASHE was coupled to the HEC linear alternator and tested as an integrated unit. The integration of the TASHE and the alternator consisted of simply bolting the two compressor/alternator halves to the TASHE centerplate. A simple mounting scheme allowed bench top operation, as shown in Figure 13. The heater power supply, load resistor bank, interlocks and data acquisition were housed in two adjacent electronics racks. The test facility is shown in Figure 14.

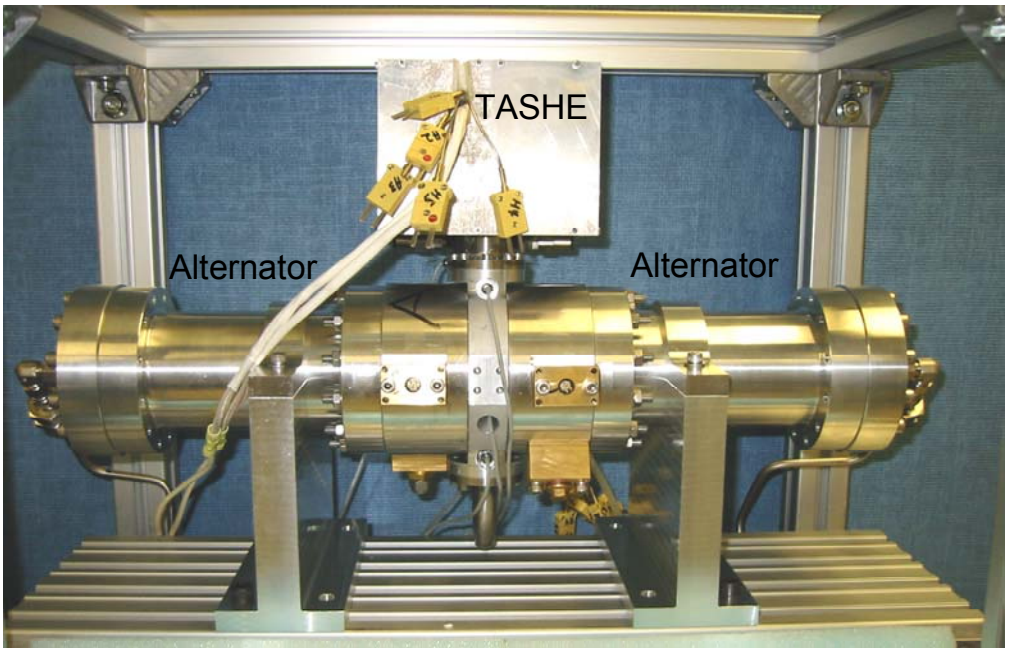

Figure 13. Thermoacoustic Heat Engine & Linear Alternator Integrated System

Figure 14. Thermoacoustic Heat Engine & Linear Alternator Test Facility

A simple passive load circuit was developed to manually control the electrical output and the stroke of the alternator. The load circuit consisted of a bank of four 16-Ohm, high-power, low-inductance rheostats to dissipate the electrical energy. In series with the load rheostats were a pair of back-to-back Zener diodes that allowed a simple passive PWM of the load such that the load's electrical dissipation increased more rapidly with stroke than the alternator's power output. It was found that a small Zener value (6V Zener out of 60 Vrms) allowed the load's power *vs.* voltage slope to be sufficiently steeper than the alternator's power *vs.* voltage (which is proportional to stroke) to allow stable manual stroke control.

The integrated unit self started when the hot end temperature exceed approximately 400 ^{o}C. In order to insure controlled conditions upon self starting, the load resistance was kept very low during the warm up of the hot end by using a 2-Ohm crowbar across the alternator coils. This prevented the alternator from oscillating. When the hot end was at the desired temperature, the load resistors were set to zero Ohms and the crowbar load was removed. The load resistance was gradually increased until the unit self-started and further increased while monitoring the alternator stroke on an oscilloscope until the desired stroke was obtained. To protect against inadvertent over stroking of the alternator, the alternator stroke signal was fed into a comparator that activated a latching relay to connect the 2-Ohm crowbar load across the alternator coils if the stroke signal exceeded safe limits.

In order to allow the dc piston position to be adjusted, an external dc-offset control circuit allowed injection of dc current into the alternator coils, but not into the load. This circuit consisted of a manually adjusted dc voltage signal that controlled a current-mode amplifier that produced a dc-current output. The load resistor bank had a pair of low-ESR capacitors in series with it to block the dc current from flowing into the load. A separate power meter allowed the power input from the external circuit to be monitored. The external position control circuit could be switched in and out of the load circuit completely. The load circuit with the optional dc position control circuit is shown in Figure 15.

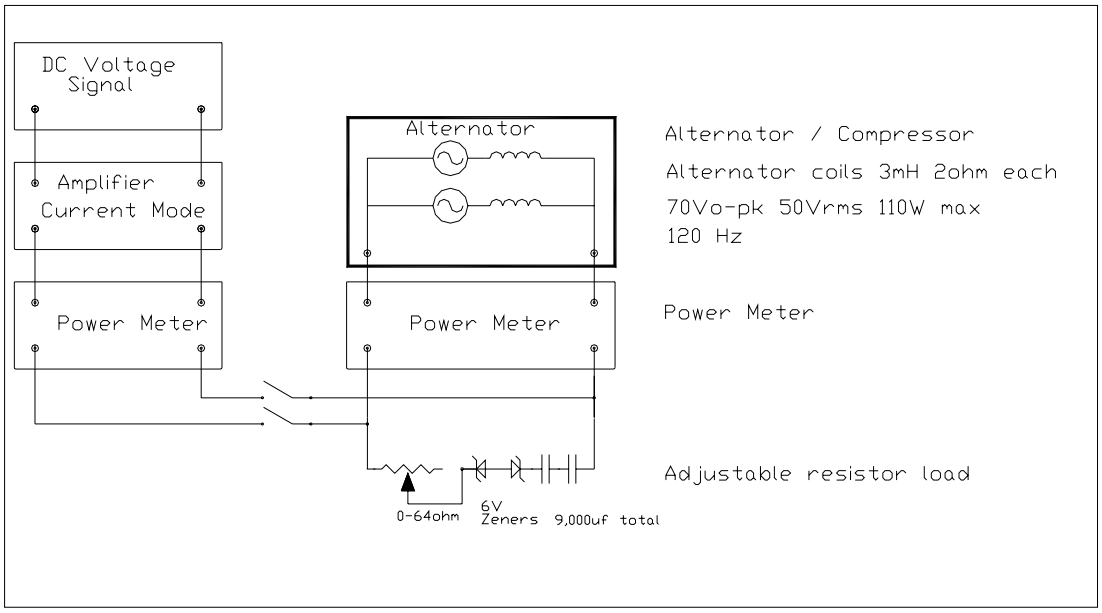

Figure 15. Load circuit for Thermoacoustic Heat Engine & Linear Alternator

Integrated TASHE/Alternator Test Results

The power converter performance was characterized as a function of heat input (and thus alternator stroke) at fixed hot-end temperature and fixed reject temperature. Additional characterization was done varying reject temperature while maintaining fixed hot-end temperature and fixed alternator stroke.

The ac electrical power output *vs.* stroke at fixed T_{reject}=28 ^{o}C is shown in Figure 16 along with the DeltaE modeled power output. At the maximum stroke tested, the ac electrical power output was 57 W with 377 W net heat input.

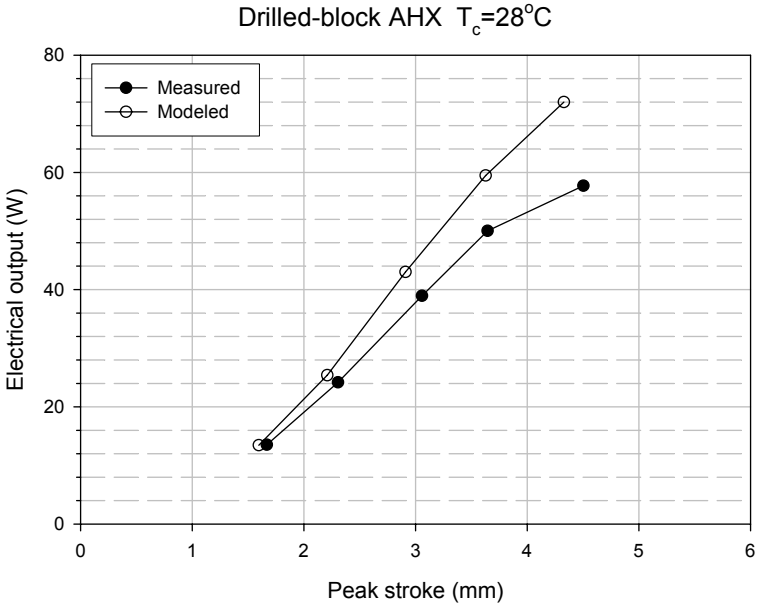

Figure 16. AC Electrical power output vs. stroke at fixed T_{reject}=28 °C

The system efficiency (ac electrical power out per net heat in) as a function of stroke at fixed T_{reject}=28 °C is shown in Figure 17. At its most efficient point, the system efficiency was 17.8 % and the ac electrical power output was 39 W

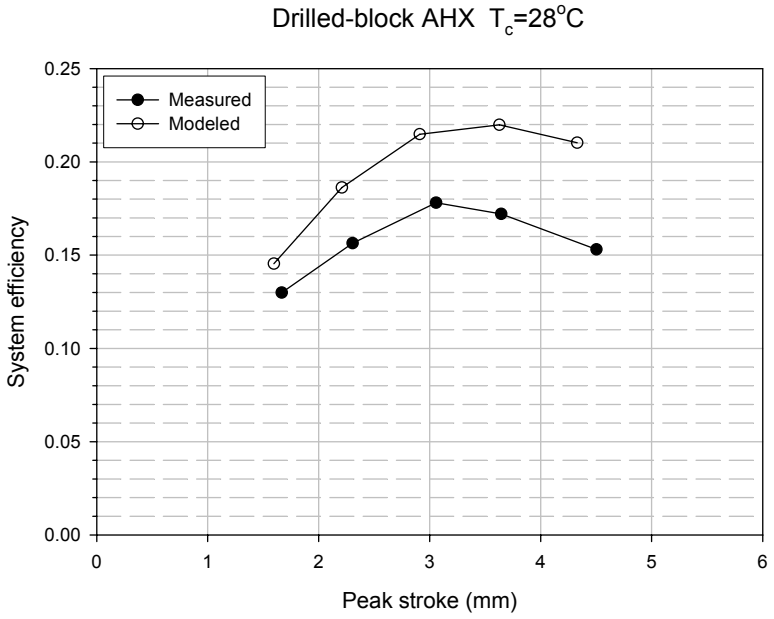

Figure 17. Efficiency (AC Electrical power output per net heat input) vs. stroke at fixed T_{reject}=28 °C

The TASHE used in this testing was optimized at a reject temperature of ~10 °C for ease of laboratory testing. It was tested over a range of reject temperatures up to 80 °C, as shown in Figure 18. As expected, the power and efficiency dropped with increasing reject temperature. To investigate what could be expected had this hardware been optimized at 80 °C, the geometry in the DeltaE model was re-optimized at a reject temperature of 80 °C. This improves the predicted

performance at 80 °C as shown by the open triangles in Figure 18. The changes to the TASHE model include a different regenerator screen pack, compliance volume, and inertance length. These are all changes that could fairly easily be done on the current hardware.

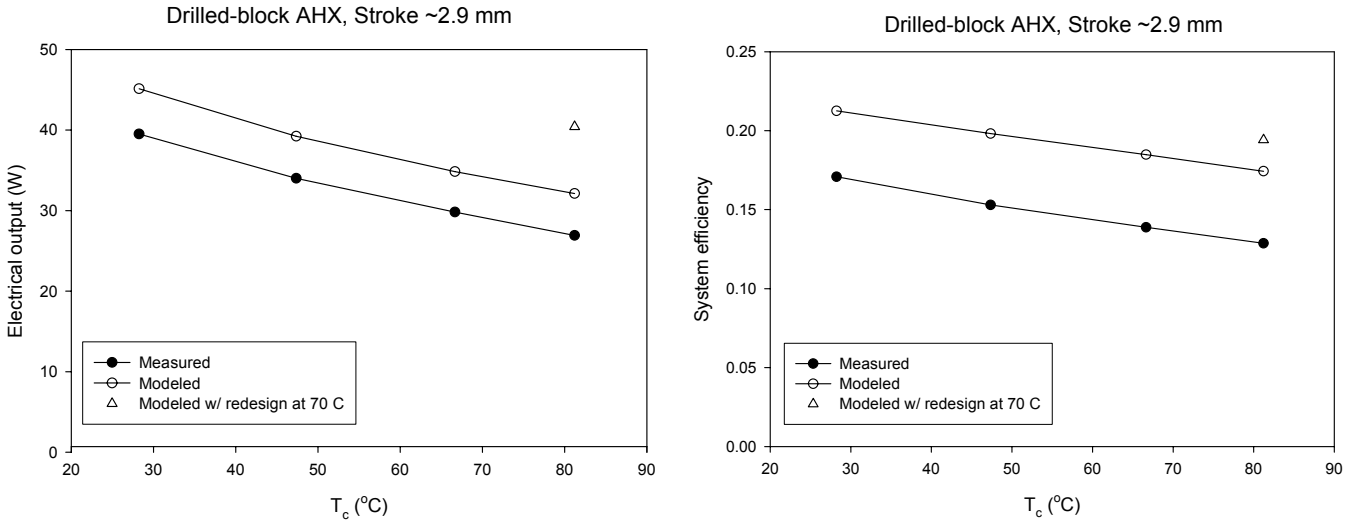

Figure 18. Re-optimization of the TASHE model at a reject temperature of ~80°C improves the predicted performance at 80 °C

Discussion of Test Results

There were many additional measurements and analyses to validate the system-level data, to determine where there is room for future improvement, to anchor future modeling, and to insure that the hardware was operating properly. First, the temperature distribution in the TASHE is measured to make sure the jet pump is adequately suppressing the parasitic streaming. The temperature distributions in Figure 19 show the proper linear temperature profiles for the variable-stroke, fixed-T_{reject} testing. This data also provides the regenerator hot and ambient temperatures (at x=0 and x=1) that are used as inputs to the DeltaE modeling of the tests results.

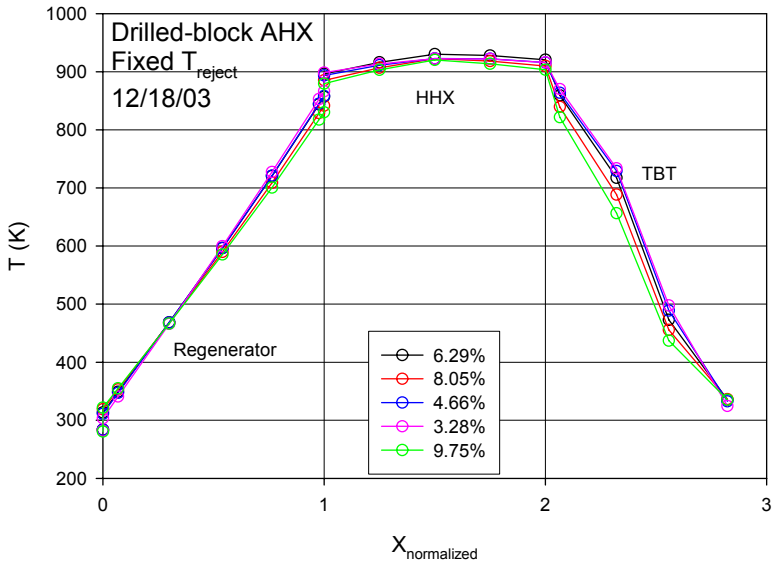

Figure 19. Temperature profile in TASHE during operation with the linear alternator.

The pressure drops across various components in the TASHE are shown in Figure 20 and compared with their modeled values. The isolated red circle shows the case when a screen-packed ambient heat exchanger (AHX) was used in place of the drilled-block AHX. The pressure drop across the "regenerator" which includes the AHX pressure drop, is significantly higher with the screen-packed AHX. To significantly improve the future performance of the AHX, a better geometry, such as parallel plates, is likely needed.

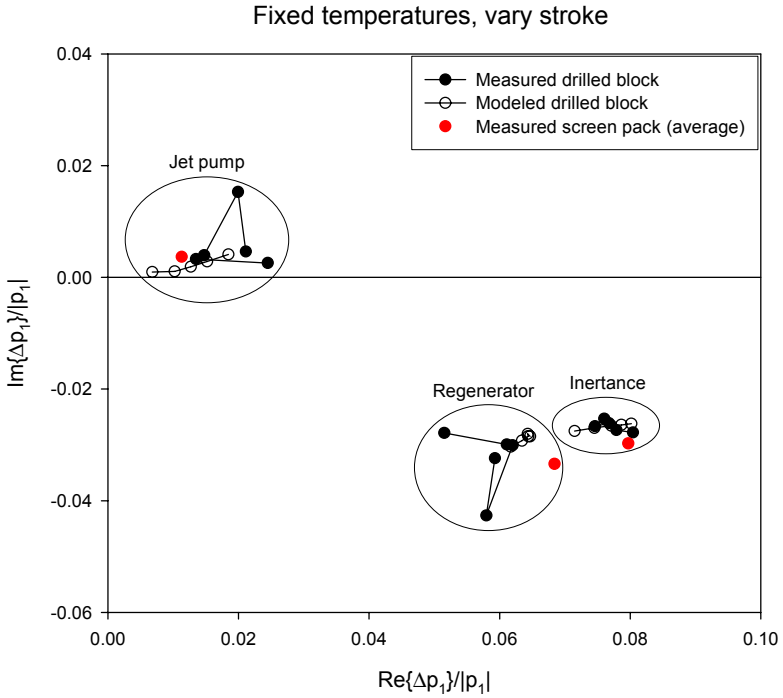

Figure 20. TASHE pressure drops when operating with linear the alternator

A key reality check is whether DeltaE and measurement agree on the alternator stroke as a function of the pressure amplitude in the TASHE. Figure 21 shows the good agreement between model and measurement.

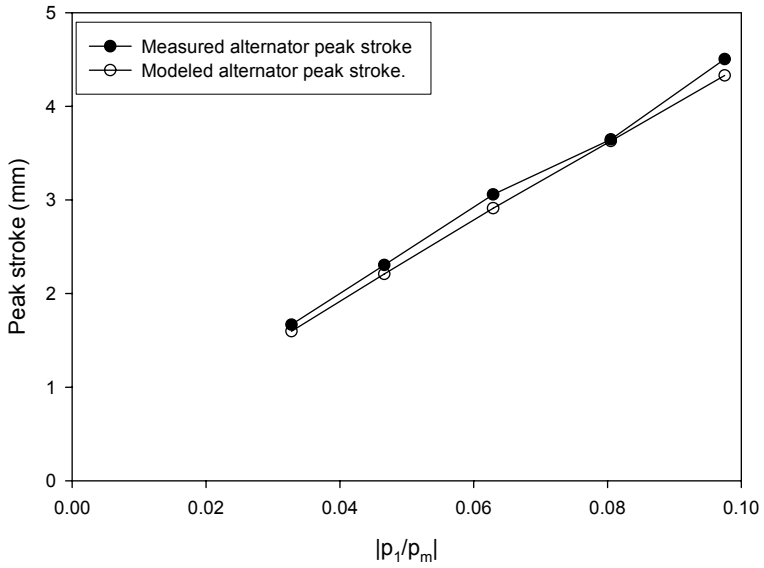

Figure 21. Stroke vs. pressure amplitude measured vs. modeled

In addition to temperature profiles, pressure drops, and volumetric flow rates, the acoustic power in the compression space was also measured using the flush-mounted pressure transducer and the piston position obtained from the LVDT sensors. Sensitive phase measurements were obtained with a lock-in amplifier. Careful phase calibrations of the LVDT and pressure transducer allowed the small phase angle to be accurately measured. The measured acoustic power is delivered to an imaginary surface located just in front of the pistons. Losses in the seals, motor, and pressure vessel surfaces subtract from the shaft power delivered to the piston. The losses in the compression space and plumbing to the compression space are included in the TASHE loss budget. With good agreement in the pressure drops and alternator stroke, the good agreement in acoustic power output as shown in Figure 22 is expected.

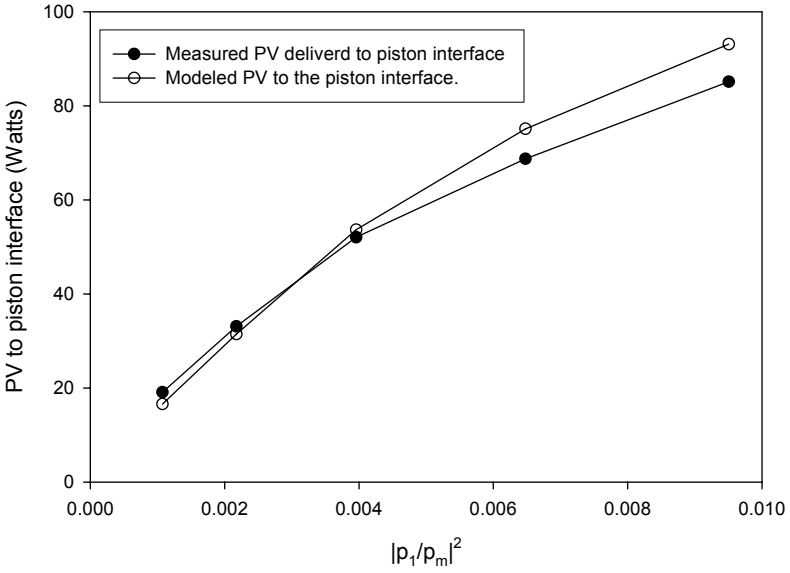

Figure 22. Acoustic power delivered to the piston face, measured vs. modeled

Since the acoustic powers are in good agreement with the model, the temperature profiles are reasonable (indicating no significant streaming), and we have accounted for the usual heat leaks accurately, the net heat into the TASHE should be in good agreement, as shown in Figure 23. The phase between p_1 and U_1 in the TBT show that there should be some streaming there, and crude estimates of the heat carried by this streaming are inline with the discrepancy between the model and measurements. In future efforts, the TBT should be tapered in an attempt to suppress TBT streaming.

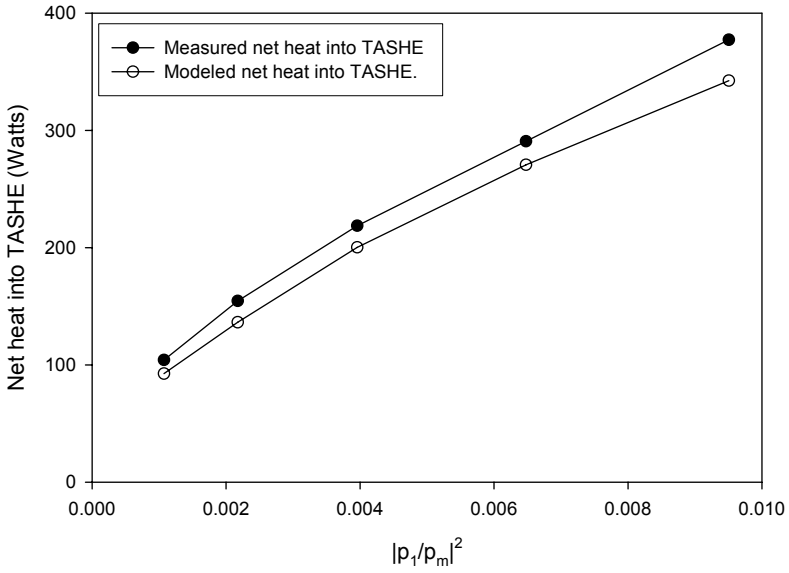

Figure 23. Net Heat into TASHE

The TASHE thermal-to-acoustic power conversion efficiency plotted in Figure 24 shows the cumulative effect of the acoustic power shortfall and the excess heat input. Overall, the measured efficiency peaks out at around 24%, which is respectable for this first effort at such a small power capacity.

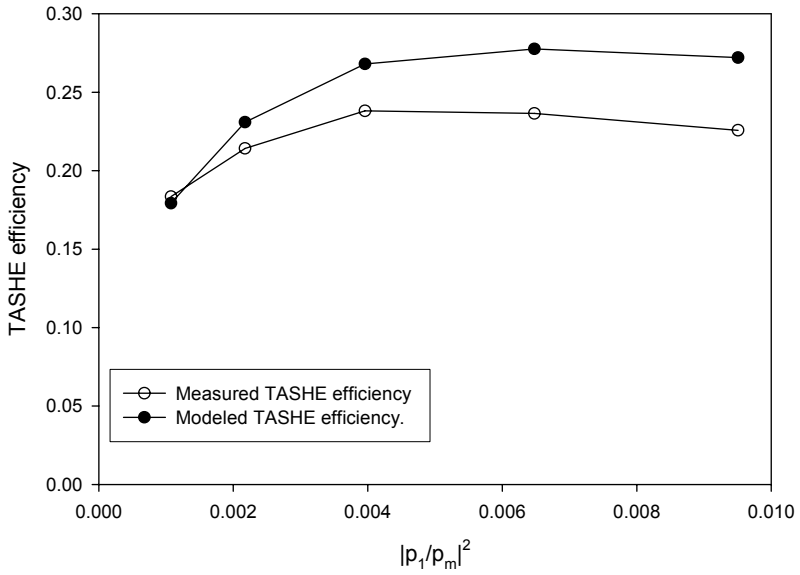

Figure 24. TASHE Efficiency (Acoustic power output/ heat input)

Throughout the testing above, the reject heat exchanger was kept near ambient temperature. In space applications, the reject temperature is bound to be higher due to constraints on radiator size. To explore the effect of higher reject temperatures, a set of measurements was taken near the amplitude where we achieved the highest efficiency in the previous testing ($|p_1/p_m|$~6.5% and a stroke of 4.1 mm). The measured acoustic power output and TASHE efficiency, along with the model results, are shown in Figures 25 and 26.

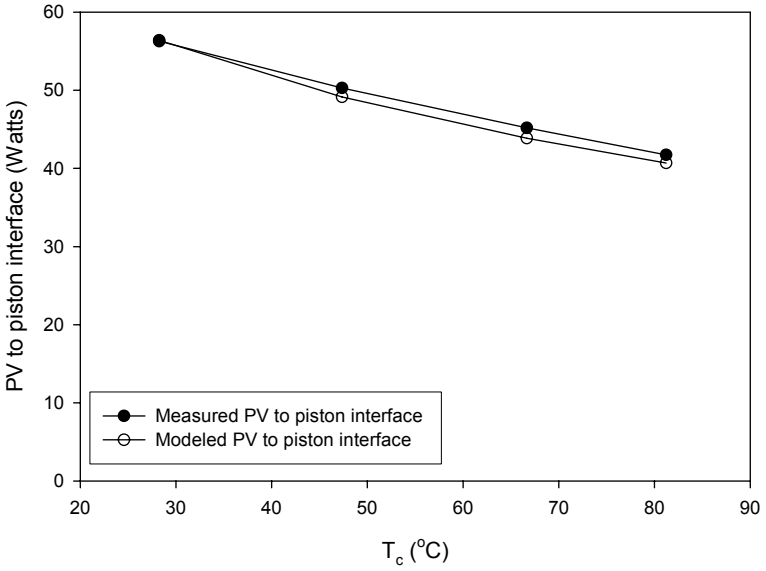

Figure 25. Acoustic power delivered to the piston *vs.* reject temperature

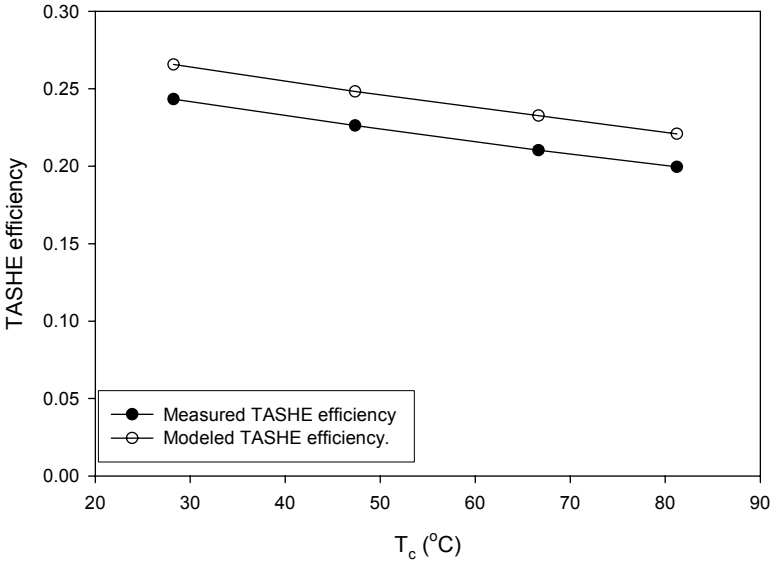

Figure 26. TASHE Efficiency (Acoustic power output/net heat input) as a function of reject temperature

Since the DeltaE model uses the hot and ambient regenerator face temperatures as inputs, the temperature drops between the heat exchanger metal and the regenerator face are results that can be compared with measurement. Since the OD of the AHX is essentially bathed in water, the surface temperature of the outside of the AHX is probably fairly constant. There is no thermocouple located directly on the OD of the AHX, but there is one located close by on the compliance shell. This thermocouple may be reading somewhat higher than the OD of the AHX, and this may be the cause of the low values of the measured ΔT's in Figure 27 below.

The HHX has a significant temperature change along its length, so it is not clear where to measure the metal temperature. We have chosen the first thermocouple station after the hot face of the regenerator as representative of the HHX metal temperature. The measured ΔT's are 15-20 ^{o}C higher than the modeled ΔT's. In any future design, the temperature variation along the HHX metal should be taken into account since the temperature limit is determined by the maximum HHX metal temperature.

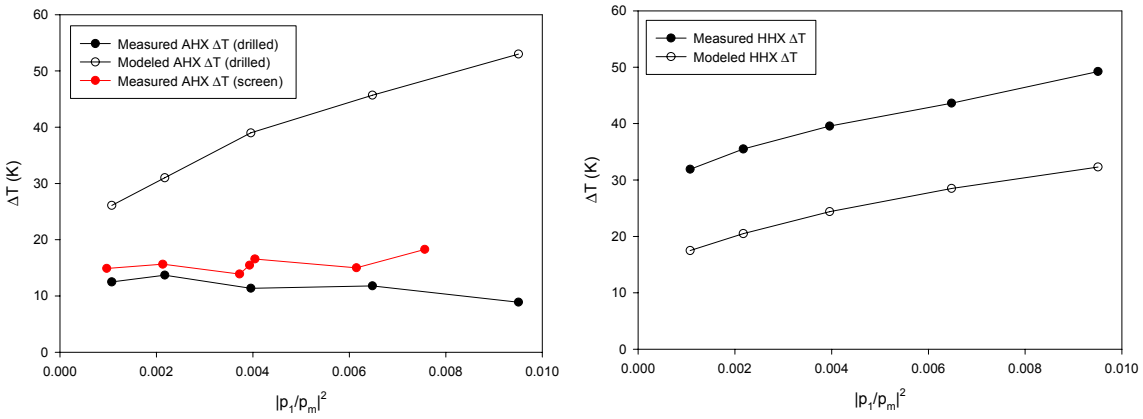

Figure 27. a) AHX and b) HHX ΔT

Next, we turn to an analysis of the alternator. Figure 28 shows the measured total acoustic power input from the TASHE to the alternator interface, the various loss mechanisms, and the measured electrical power output. The difference between the electrical power output and the acoustic power is due to losses in the alternator, which are presented in Figure 28. The alternator loss terms are all about the same size. The alternator losses at the maximum tested stroke amplitude are detailed in Table 1.

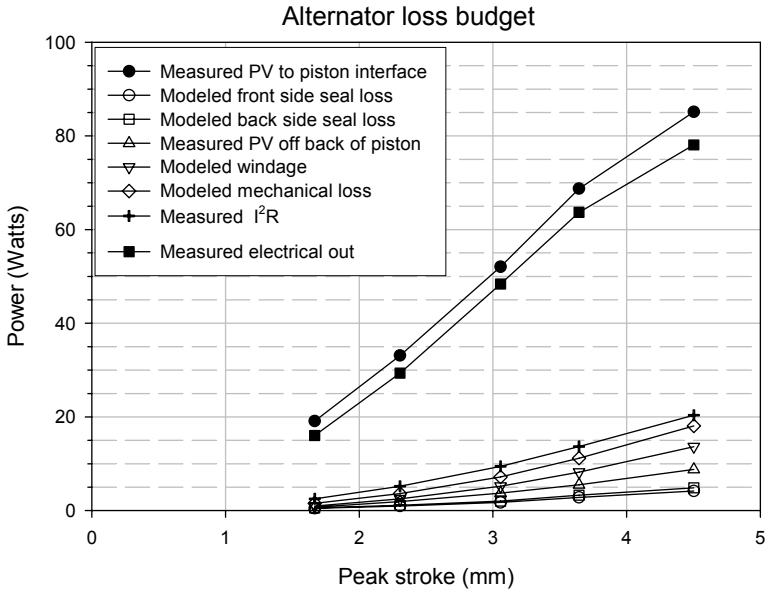

Figure 28. Alternator losses

Alternator peak stroke	4.5	mm	
Total PV deliverd to piston interface	85.1	W	
2X Side A seal loss originating from the front	4.2	W	4.9%
2X Side A seal loss originating from the back	0.7	W	0.8%
2X PV from the back of A	4.6	W	5.4%
2 X Edissipated in coil A (I^2R)	2.3	W	2.7%
2 X modeled windage loss of side A	4.8	W	5.7%
2 X R_m u^2	4.4	W	5.2%
Total electrical from motor	57.7	W	
Accounted for alternator loss	20.3	W	23.9%
Missing alternator loss	7.1	W	8.3%
Total alternator loss	27.4	W	32.2%
Alternator efficiency	68%		

Table 1. Alternator losses

Figure 29 shows the total measured alternator loss and the unaccounted alternator loss. Approximately 75% of the alternator loss is known and modeled. The origin of the remaining 25% of the total loss is unclear, but it is in rough agreement with the findings of the Oxford dead volume tests. To date, the dead volume tests are the best estimator of the total electro-acoustic conversion losses in the alternator. In future work, it will be essential to determine the origin of the unaccounted loss in the alternator so that they can be eliminated or minimized.

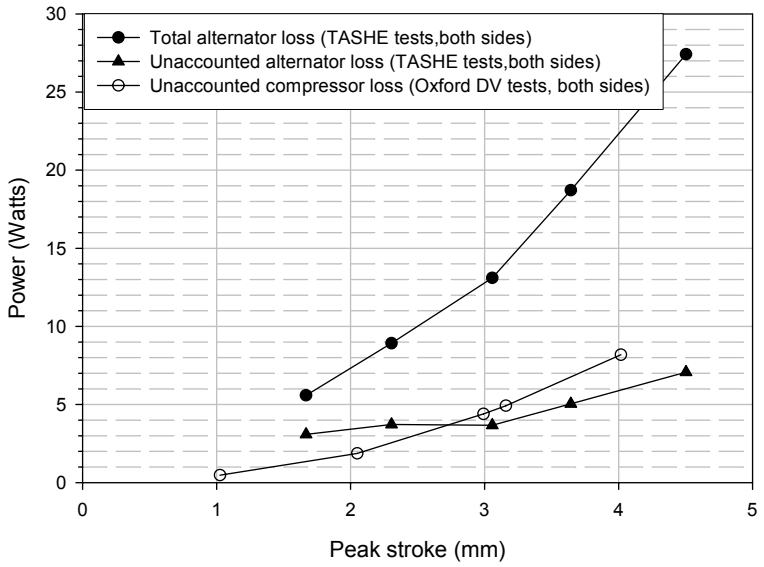

Figure 29. Total alternator loss *vs.* stroke, unexplained loss portion during TASHE-Alternator tests compared to unexplained portion during dead volume tests

Figure 30 shows the alternator "efficiency" obtained in conjunction with this TASHE. The useful information, alternator loss versus stroke, is in the previous plot. The "efficiency" of the alternator will change depending on how much acoustic power the TASHE delivers at a particular stroke and pressure amplitude, which is a function of the TASHE's losses and dead volume. Thus the TASHE and alternator efficiencies are actually interrelated.

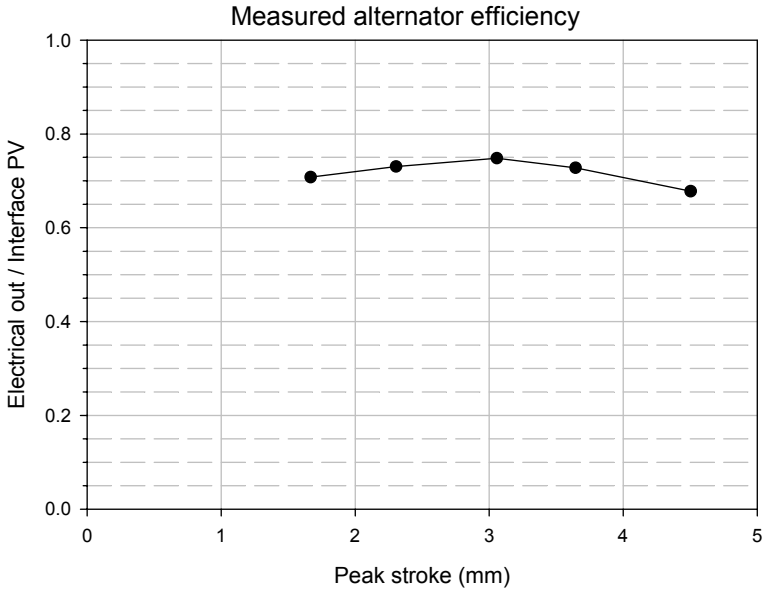

Figure 30. The alternator "efficiency" during TASHE tests. The efficiency of the alternator will change depending on how much acoustic power the TASHE delivers at a particular stroke

A review of the various losses and inefficiencies identified during the testing indicated several opportunities for system improvement. These were modeled to estimate the potential improvements, and the results are tabulated in Table 2 below.

Component improvement	System Benefit	Heat Engine Power Increase (W)	Alternator Power Increase (W)
Parallel-plate regenerator	Decrease alternator stroke by 33% Decrease alternator and flow losses	4	25
Improved ambient heat exchanger Decrease helium-to-metal temperature gap from 50ºC to 20ºC	Increased temperature difference across regenerator. Increased output power	7	5
Improved hot-heat exchanger Decrease helium-to-metal temperature gap from 50ºC to 25ºC Increase GPHS coupling area by 1.5	Increased temperature difference across regenerator. Increased output power Increased efficiency	2	1.5
Reduced TBT volume	Decrease alternator stroke by 15% Decrease alternator and flow losses	0	5
Tapered TBT	Reduce streaming heat loss	6	0
Reduce compression space volume	Reduce dead volume	0	10
Reduce surface-area-to -volume in alternator pressure vessel	Reduce gas thermal hystersis	0	3
Reduce alternator hystersis	Reduce eddy current loss	0	3

Table 2. Potential system improvements.

New Technology

The work under this contract did not result in any known patentable or nonpatentable innovations reportable under NF1679. Instead, this contract simply demonstrated that existing 1kW traveling

wave thermoacoustic engine technology could be scaled to the 100 Watt range, and that by coupling such a 100 Watt class traveling wave thermoacoustic engine to a linear alternator an efficient thermal-to-electric converter could be produced. Although significant engineering hurdles had to be overcome to produce this working thermal-to-electric demonstrator, they are in the final analysis simply engineering optimizations rather than fundamental innovations.

Conclusion

A proof-of-concept thermoacoustic power converter was modeled, designed, assembled and tested. It performed substantially as modeled. Most of the key losses in the system were identified. A conceptual design of a flight-like system was produced that indicates that a low-mass, high-efficiency, large specific-power thermoacoustic power converter is feasible for space applications.

References

Backhaus, S., and Swift, G. W., "A Thermoacoustic-Stirling Heat Engine: Detailed Study," Journal of the Acoustical Society of America, **107**, 3148-3166, 2000.

Backhaus S.,. Tward E, and Petach M., "Thermoacoustic Power Systems For Space Applications." *Proceedings of the Space Technology and Applications International Forum 2002*, edited by M. S. El-Genk, pg. 939-944, New York, NY, 2002. Springer-Verlag.

Backhaus S. "Initial Tests Of A Thermoacoustic Space-Power Engine." In these proceedings, *Space Technology and Applications International Forum, STAIF 2003*. AIP, New York, 2003.

Boldea, I., and Nasar, S. A., "Linear Electric Actuators and Generators" pg 232-233, Cambridge University Press, Cambridge U.K. 1997

Cockfield R.D. and Chan T.S., "Stirling Radioisotope Generator for Mars Surface and Deep Space Missions," Proceedings of IECEC 2002 Conference. Paper # 188, 2002.

Mondt, J. F., "Advanced Radioisotope Power System Technology Developments for NASA Missions 2001 and Beyond," Proceedings of the IECEC, 133-139, Savannah, GA, August, 2001.

Tward, E., Chan, C.K., Jaco, C., Godden, J., Chapsky, J. and Clancy, P., "Miniature space pulse tube cryocoolers", Cryogenics 39, pp 717-720 (1999)

Tward , E., and Davis, T., "High Efficiency Cryocooler", #99-4564, AIAA Albuquerque, Sept. 1999

Tward, E., Chan, C.K., Colbert, R., Jaco, C., Nguyen, T., Orsini, R., and Raab, J., "High Efficiency Cryocooler," Cryocoolers 11, R. Ross ed., Kluwer Academic/Plenum Publishers, 2001.

Ward, W. C., and Swift, G. W., "Design Environment for Low Amplitude Thermoacoustic Engines, DeltaE," Journal of the Acoustical Society of America, **95**, 3671-3672, 1994. Fully tested software and users guide available from Energy Science and Technology Software Center, US Department of Energy, Oak Ridge, Tennessee. To review DeltaE's capabilities, visit the Los Alamos thermoacoustics web site at http://www.lanl.gov/projects/thermoacoustics/

Appendix A. TASHE Hot End Stress Analysis

An FEA analysis of the current, demonstrated TASHE hot end indicates that it should meet the 100,000-hour durability requirement when made from Inconel 718. An ANSYS finite-element analysis of the stresses in the TASHE hot end under operating conditions, in conjunction with the measured operating temperatures (Figure 1) allows the stress *vs.* temperature at key locations to be compared to the durability requirement. The 100,000-hour durability requirement has been defined by GRC in Halford et al[1] and by Shreiber[2] as 99.99% reliability to greater than 100,000 hours until onset of tertiary creep. We used the methodology of Halford to determine a maximum stress *vs.* temperature curve for thin Inconel 718 corresponding to this requirement. We used the ORNL creep–rupture law

$$\log(t_r) = C_h + C_1 \log\sigma + C_2(\log\sigma)^2 + C_3(\log\sigma)^3 + C_4 T \log\sigma$$

and the constants in Hanford's paper to obtain a curve for the 50% PoS time-to-rupture curve for the ORNL thick sample data at 650 ^{o}C. Then, a curve fit for the GRC thin sample data was obtained by adjusting C_h, following Halford. We then further adjusted C_h to get the suggested estimate of 50% PoS time to onset of tertiary creep, again following Halford. An additional factor of 2 reduction in stress, based on Table III of Halford, was used to get the stress at 99.99% PoS from the stress at 50% PoS. This is shown in Figure 2. The ORNL creep-rupture law has thus been recast as a creep-durability law based on the GRC durability definition above. This provides an allowable maximum stress *vs.* temperature curve, which corresponds to the durability requirement. The calculated stress *vs.* measured temperature for the operating conditions of the TASHE are compared to the allowable stress *vs.* temperature in Figure 3. It is apparent that the TASHE as built and tested would meet NASA GRC's durability requirement when made from Inconel 718. Additional margin, although not required, could be obtained with no performance penalty by a minor increase in the diameter of the columns connecting the top and bottom plates of the TASHE hot HX

[1] "Structural Analyses of Stirling Power Converter Heater Head for Long Term Reliability, Durability and Performance" NASA/TM-2002-211327, Halford G.R., Shah, A., AryaV.K., Krause,D.L. and Bartolotta, P.A.

[2] Personal communication from Jeffrey G Schreiber, 5/2/03

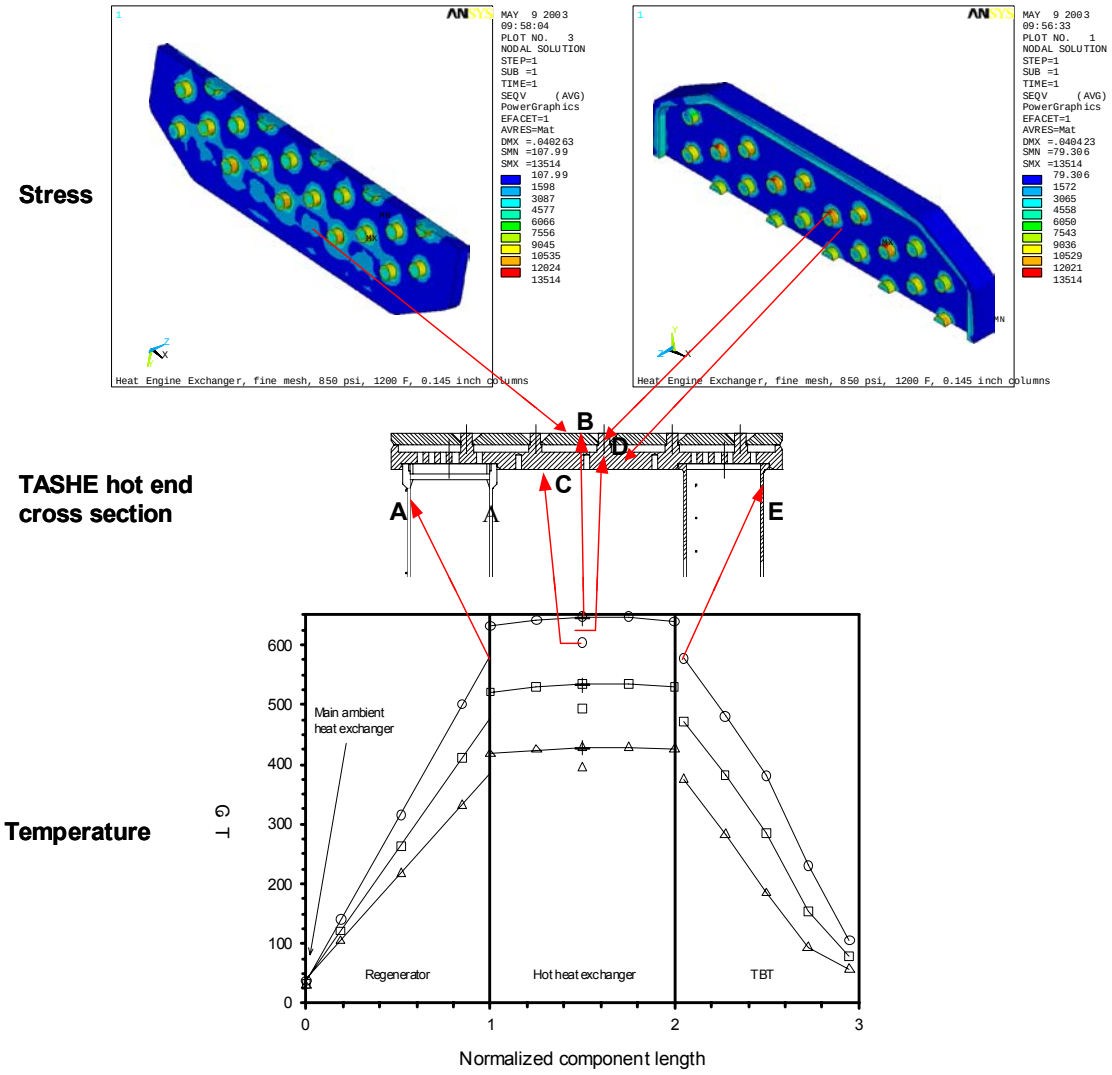

Figure A1. FEA analysis of the combined pressure and thermal stress in the TASHE hot end, using the peak pressure and the measured temperature distribution, allowed stress *vs* temperature in the TASHE components to be compared to durability requirements

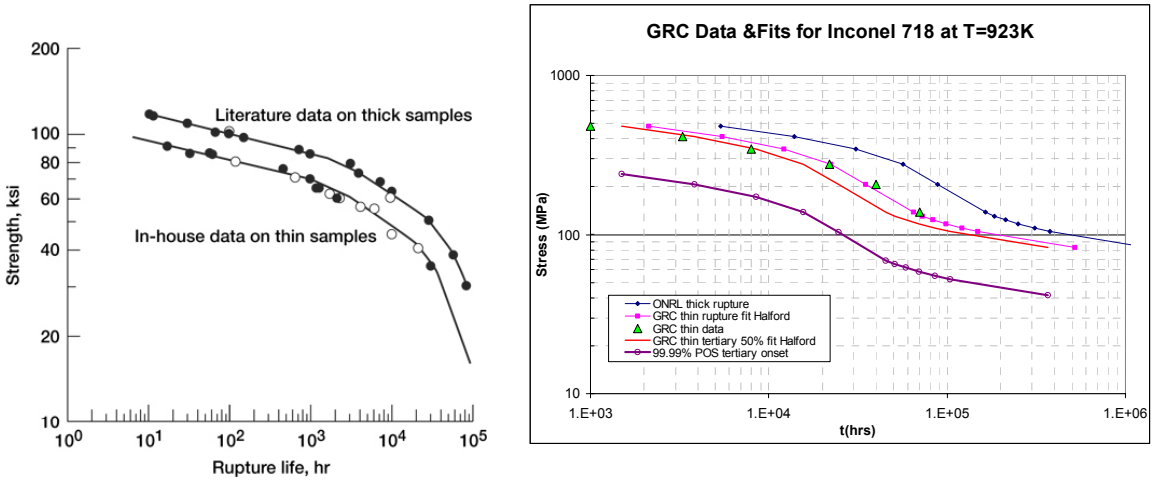

Figure A2. Existing data from NASA GRC for thin Inconel 718 samples at 650 ^{o}C allows the durability requirement (100,000 hours till onset of tertiary stress with 99.99% probability of success) to be plotted as a function of stress. The NASA GRC curve-fit methodology also allows maximum stress *vs* temperature to be curve fit

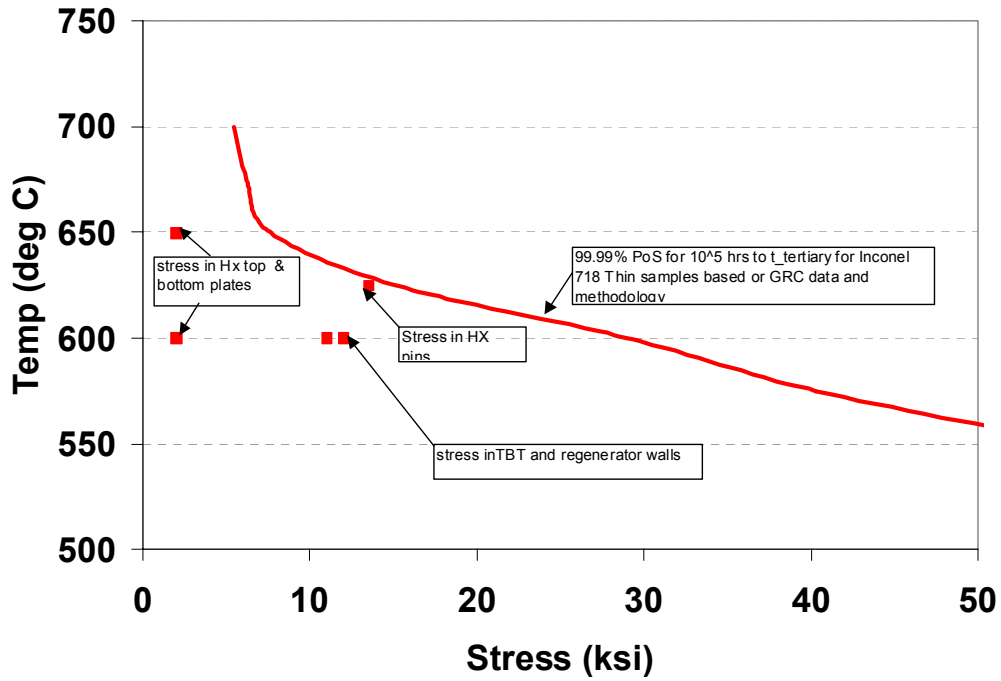

Figure A3 The calculated stresses at several key locations in the operating TASHE are plotted *vs* the measured temperature. The data are compared against the stress vs temperature curve that corresponds to NASA GRC's durability requirement. The TASHE as built and tested would meet NASA GRC's durability requirement when made from Inconel 718

Appendix B. Alternator Materials Compatibility Matrix

Candidate replacement materials have been identified as being acceptable in the harsh Europa radiation environment.

- **NdFeB Magnet Assessment (Lockheed Martin) December 16, 1999**

LMA has concluded that the Europa radiation environment will produce insignificant changes in the Nd-Fe-B magnetic materials.

- **Organic Materials Radiation (GRC, others) Updated as of January 11, 2000**

Old Material	Location	Purpose	New Material/ Mission Rating
Xylan 1620-560 Blue	Piston OD	Bearing Coating	Xylan 1054 1
Polyimide (Kapton)	Wire Insulation	Wire Insulation	Acceptable as is 1
Dolph CB-1057 Epoxy	Coils	Bonding Agent	EC2216 1
Loctite 420	Stator laminations	Wicking Adhesive	Loctite 4014 or Epotek 301 2
Scotch-weld DP-460	Magnets, Stator	Epoxy Adhesive	EC2216 1
3M heat shrink tubing	Wire connectors	Electrical Insulation	Raychem PVDF 1
Kapton tape (KA00)	Edge of Stator	Electrical Wire Protection	Permacel or 3M Y966 1
Garolite G-10	Coils, Laminates	Electrical Insulation	Acceptable as is 1
TFE Insulation	Wires for Feed Through	Electrical Insulation	Raychem PVDF 1
TFE Structure	End of Piston	Power Piston Bumper	PVDF or EFTE machined 1

***Mission Rating:**
1 = Current materials acceptable
2 = Acceptable; requires dose calculations
3 = Acceptable, with dose calculations & test data
4 = Questionable; conclusive proof required
5 = Unacceptable